the 40 days studied, and HIV-specific antibodies are detectable in the animals with high plasma viral loads and HIV-DNA copy numbers, we also discuss the suitability of HIV-hNOG mice as an animal model for HIV-1 infection.

## Materials and methods

### Transplantation of human CB-derived hematopoietic stem cells in NOG mice

Human cord blood (CB) was obtained from Saiseikai Central hospital (Minato-ku, Tokyo, Japan) and Tokyo Cord Blood Bank (Katsushika-ku, Tokyo, Japan) after obtaining informed consent. All research on human subjects was approved by the Institutional Review Board of each institution participating in the project. CB mononuclear cells were separated by Ficoll-Hypaque density gradient. $CD34^+$ hematopoietic stem cells were isolated using a magnetic-activated cell sorting (MACS) Direct CD34 Progenitor Cell Isolation Kit (Miltenyi Biotec, Bergisch Gladbach, Germany) according to the manufacturer's instructions. More than 95% of $CD34^+$ cells were positively selected after 2 time-enrichment manipulations. Cells were either immediately used for the transplantation or frozen until use. NOG mice were obtained from the Central Institute for Experimental Animals (Kawasaki, Japan) and maintained under specific pathogen-free (SPF) conditions in the animal facility of the National Institute of Infectious Diseases (NIID; Tokyo, Japan). Mice used in these studies were free of known pathogenic viruses, herpes viruses, bacteria, and parasites. They were housed in accordance with the Guidelines for Animal Experimentation of the Japanese Association for Laboratory Animal Science (1987) under the Japanese Law Concerning the Protection and Management of Animals, and were maintained in accordance with the guidelines set forth by the Institutional Animal Care and Use Committee of NIID, Japan. Once approved by the Institutional Committee for Biosafety Level 3 experiments, these studies were conducted at the Animal Center, NIID, Japan, in accordance with the requirements specifically stated in the laboratory biosafety manual of the World Health Organization. Female mice (6 to 10 weeks old) were irradiated (300 cGy) and $1 \times 10^4$ to $1.2 \times 10^5$ $CD34^+$ cells were intravenously injected within 12 hours.

### Flow cytometry

The purity of CB-derived $CD34^+$ cells after separation was evaluated by double staining with FITC-conjugated anti–human CD45 (J.33) and PE-conjugated anti–human CD34 (Class III 581) (all from Beckman Coulter, Fullerton, CA). After transplantation (1-7 months), peripheral blood, spleens, bone marrow (BM), and thymi were collected for flow cytometric analysis following staining with the following monoclonal antibodies (mAbs): FITC-conjugated anti–human CD45 (J.33), CD3 (UCHT1), CD4 (13B8.2), CD19 (J4.119), CD45RO (UCHL1) (all from Beckman Coulter), and CCR5 (2D7; BD Pharmingen, San Diego, CA); PE-conjugated anti–human CD4 (13B8.2), CD8 (B9.11), CD19 (J4.119), CD45RA (ALB11) (all from Beckman Coulter), and CXCR4 (44717; R&D Systems, Minneapolis, MN); anti–mouse CD45 (YW62.3; Beckman Coulter); ECD-conjugated anti–human CD45 (J.33; Beckman Coulter); and PC5-conjugated anti–human CD8 (T8) and CD14 (Rm052) (all from Beckman Coulter). Flow cytometric analysis was conducted by 2- or 4-color staining using an EpicsXL (Beckman Coulter).

### Immunohistochemistry

Organs were snap-frozen following embedding in OCT compound (Sakura Finetechnical, Tokyo, Japan). Frozen sections were air-dried and fixed in acetone. HIV-1–infected organs were fixed in 4% paraformaldehyde and embedded in OCT compound following immersion in gradient sucrose (5%-30%). Fixed samples were stained with the following mAbs: anti–human CD45 (1.22/4014; Nichirei, Tokyo, Japan), CD3 (UCHT1; DAKO, Glostrup, Denmark), CD20 (L26; DAKO), CD68 (KP1; DAKO), CD205 (MG38; eBioscience, San Diego, CA), and DRC-1 (R4/23; DAKO) for follicular dendritic cells (FDCs); anti–mouse FDC-M1 (BD Pharmingen) for murine FDCs; and HIV-1 Gag p24 (DAKO) for detection of infected cells. Biotin-labeled goat $F(ab')_2$ anti–mouse immunoglobulin (Ig; ICN Biomedicals, Aurora, OH)– or biotin-labeled mouse $F(ab')_2$ anti–rat IgG (Jackson ImmunoResearch Laboratories, West Grove, PA) was used as the secondary antibody. Samples were treated with alkaline phosphatase (AP) or horseradish peroxidase (HRP)–streptavidin conjugate (ZYMED Laboratories Inc, San Francisco, CA). BCIP/NBT, DAB, or AEC (all from DAKO) was used for the visualization. Photographs were taken by light microscopy (Leica DMRA; Leica Microsystems Wetzlar, Wetzlar, Germany) using Leica HC PLAN APO lenses (10×/0.40 NA PH1). Leica Q550 was used for image processing.

### Measurement of human Igs in mice plasma

Plasma concentrations of human IgM, IgG, and IgA in NOG mice that received transplants of human stem cells were determined by conventional human Ig quantitation assay at BML Inc (Tokyo, Japan).

### Cells and viruses

Human embryonic kidney 293T cells and monkey kidney COS7 cells were cultured in RPMI 1640 supplemented with 10% fetal bovine serum (FBS) and antibiotics. The 293T cells and COS7 cells were used for transfection of DNA plasmids containing $HIV\text{-}1_{JRCSF}$ and simian/human immunodeficiency virus (SHIV)–C2/1, respectively. The SHIV-C2/1 strain contains the *env* gene of pathogenic HIV-1 strain 89.6.[19] Cell-free supernatant was collected and stored at −80°C before use. A primary clinical isolate, $HIV\text{-}1_{MNp}$, was kindly provided by Dr J. Sullivan of the University of Massachusetts Medical School (Worcester, MA). PBMCs isolated from HIV-1–seronegative individuals were cultured in RPMI 1640 supplemented with 10% FBS and antibiotics with 5 μg of phytohemagglutinin (PHA)/mL for 3 or 7 days (PHA-PBMCs). $HIV\text{-}1_{MNp}$ was propagated in PHA-PBMCs, and cell-free virus stocks were stored at −80°C.

The 50% tissue-culture infectious dose ($TCID_{50}$) was determined using PHA-PBMCs and the endpoint dilution method. A 4-fold series of dilution was prepared from the virus stock, and then cells were mixed and cultured for 7 days for X4–HIV-1 and 14 days for R5–HIV-1 in RPMI 1640 supplemented with 20% FBS and antibiotics. The endpoints were determined by screening for the p24 antigen using Lumipulse (Fujirevio, Tokyo, Japan).

### HIV-1 infection

All procedures for the infection and maintenance of NOG mice were performed in Biosafety Level 3 facilities at NIID under standard caging conditions. On days 102 to 132 after stem cell transplantation, 16 mice were inoculated intravenously with R5-tropic $HIV\text{-}1_{JRCSF}$ (65 000 $TCID_{50}$) or X4-tropic SHIV-C2/1 (50 000 $TCID_{50}$). On days 18 to 43 after inoculation, plasma was collected to determine HIV-RNA copy numbers, and spleen cells were prepared as single-cell suspensions to analyze the CD4/CD8 ratio using flow cytometry. A number (14) of other mice were inoculated intravenously with R5-tropic $HIV\text{-}1_{JRCSF}$ (200 or 65 000 $TCID_{50}$) or X4-tropic $HIV\text{-}1_{MNp}$ (180 or 20 000 $TCID_{50}$) on days 126 to 146 after transplantation. On days 18 to 40 after inoculation, plasma was collected for the determination of HIV-RNA copy numbers, and single-cell suspensions of the spleen, BM, and thymus were prepared for HIV-DNA measurement. The CD4/CD8 ratio in the spleen and percentages of human $CD45^+$ cells in organs were analyzed using flow cytometry.

### Virologic analysis

Plasma viral RNA copy numbers were measured using a real-time quantification assay based on the TaqMan system (Applied Biosystems, Foster City, CA). Plasma viral RNA was extracted and purified using a QIAamp Viral RNA Mini Kit (Qiagen, Valencia, CA). The RNA was subjected to reverse transcription (RT) and amplification using a TaqMan One-Step RT–polymerase chain reaction (PCR) Master Mix Reagents Kit (PE Biosystems, Foster City, CA) with HIV-1 gag consensus primers

(forward, 5′-GGACATCAAGCAGCCATGCAA-3′; and reverse, 5′-TGCTATGTCACTTCCCCTTGG-3′) and an HIV-1 gag consensus TaqMan probe (FAM-5′-ACCATCAATGAGGAAGCTGCAGAA-3′-TAMRA). For SHIV-C2/1 analysis, primers (forward, 5′-AATGCAGAGCCCCAAGAAGAC-3′; and reverse, 5′-GGACCAAGGCCTAAAAAACCC-3′) and a TaqMan probe (FAM-5′-ACCATGTTATGGCCAAATGCCCAGAC-3′-TAMRA) were designed for targeting the SIVmac239 gag region.[20] Probed products were quantitatively monitored by their fluorescence intensity with the ABI7300 Real-Time PCR system (PE Biosystems). To obtain control RNA for quantification, HIV-1 gag RNA and SIVmac239 gag RNA were synthesized using T7 RNA polymerase and pKS460. Viral DNA was extracted and purified using a QIAamp DNA Mini Kit (Qiagen). Determination of HIV-1 DNA copy numbers was performed by real-time PCR assay with TaqMan Master mixture (PE Biosystems). Primers (forward, 5′-GGCTAACTAGGGAACCCACTG-3′; and reverse, 5′-CTGCTAGAGATTTTCCACACT-3′) and probes (FAM-5′-TAGTGTGTGCCCGTCTGTTGTGTGAC-3′-TAMRA) were designed for targeting the HIV-1 long terminal repeat region, R/U5. The viral DNA was quantified using LightCycler (Roche Diagnostics, Almere, The Netherlands). Viral RNA and DNA were calculated based on the standard curve of control RNA and DNA. All assays were carried out in duplicate.

### HIV-antigen ELISA

Levels of anti–HIV-1 Igs against recombinant HIV-$1_{IIIB}$ Env gp120, recombinant HIV-$1_{MN}$ Env gp120, and recombinant HIV-$1_{IIIB}$ Gag p24 (all from ImmunoDiagnostics Inc, Woburn, MA) in plasma from HIV-1–infected and –uninfected control mice were determined using a standard enzyme-linked immunosorbent assay (ELISA). Microplates (96-well) were coated overnight with 200 ng/well antigens, and plasma diluted 1:20, 1:60, and 1:180 with PBS were incubated for 1 hour. AP-labeled anti–human Igs (γ, α, and μ; Sigma-Aldrich, St Louis, MO) were used as secondary antibodies. P-nitrophenylphosphate (pNPP) Solution (WAKO Chemical USA, Richmond, VA) was used for the visualization. The enzyme reaction was stopped by addition of 0.1 M NaOH and read at 405 nm. All assays were carried out in triplicate.

### Statistical analysis

Data were expressed as the mean value ± standard deviation (SD). Significant differences between data groups were determined by 2-sample Student *t* test analysis. A *P* value less than .05 was considered significant.

## Results

### Reconstitution of human lymphoid systems in hNOG mice

The initial studies describing the construction of humanized SCID mice used the human PBMC for infection of immunodeficiency viruses.[9,12,21] However, these hu-PBL-SCID mice showed a partial infection to the R5 virus and a relatively limited period of viral replication. To construct a more suitable mouse model mimicking HIV-1 infection in humans, we selected human CB stem cells as a transplant for NOG mice. NOG mice were inoculated intravenously with human CD34$^+$ hematopoietic stem cells, and their development of human lymphoid systems were then monitored. After transplantation (2 months), human CD45$^+$ leukocytes were recognized in both PB and the spleen, but most of the cells were human B cells (Figure 1A). Human T cells began to be recognized clearly in PB and the spleen 4 months after transplantation (Figure 1B) and gradually increased in level, as did human B cells (Figure 1C).

In Figure 1D, we summarized percentages of human CD3$^+$ T cells in human CD45$^+$ cells from 38 mice from 39 to 213 days after transplantation. Human CD3$^+$ T cells clearly increased 100 days after transplantation in both PB and the spleen. After transplantation (4 months), human CD3$^+$ T cells in the spleen preferably expressed CD45RA rather than CD45RO (70.8% ± 13.4% and 27.3% ± 38.8% in CD3$^+$ T cells, respectively; n = 5; Figure 1E), demonstrating that most of the T cells were in a naive state. In addition, plasma taken from 5 mice 113 to 143 days after transplantation showed that all mice produced human IgM, with concentrations ranging from 0.025 to 0.5 g/L, and that human IgG and IgA was also detected in some of the mice (ranges, 0.015-0.18 g/L and 0.003-0.012 g/L, respectively) (data not shown).

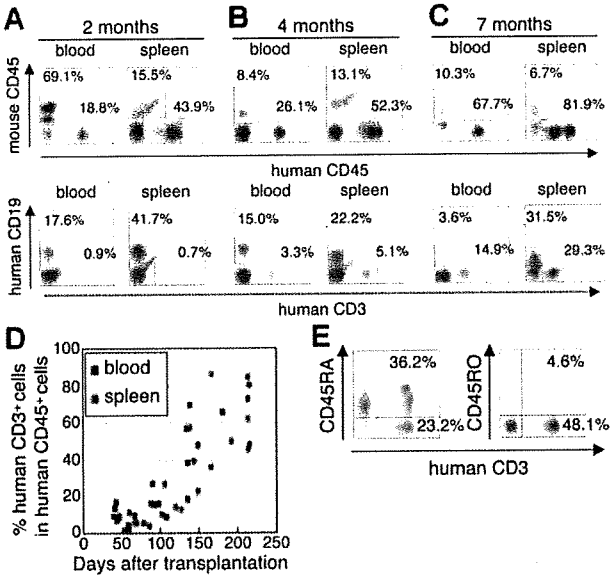


**Figure 1. Flow cytometric analysis of human T cells in the peripheral blood and spleen in NOG mice given intravenous transplants of human CB-derived CD34$^+$ cells.** (A-C) Representative profiles of the mice 2 months (A), 4 months (B), and 7 months (C) after transplantation. The ratio of human to murine CD45$^+$ cells and that of human CD3$^+$ to CD19$^+$ cells show an incremental increase in human CD45$^+$ cells and human CD3$^+$ cells from 2 to 7 months. (D) Change of net percentages of human CD3$^+$ T cells among human CD45$^+$ cells in peripheral blood and the spleen from 38 mice 39 to 213 days after transplantation. (E) CD45RA is more efficiently expressed than CD45RO on human CD3$^+$ T cells in spleen. A gate was set on the human CD45$^+$ population. The fluorescence-activated cell sorting (FACS) profile is representative of 1 in a group of 5 mice.

By 7 months after transplantation, human CD45$^+$ leukocytes comprised more than 80% to 90% of mononuclear cells in the spleen (Figure 1C), and most of the mice showed symptoms of a wasting condition and a hunched back. Based upon these results, we determined that the suitable period for HIV inoculation would be 4 to 5 months after transplantation.

### Formation of lymphoid structures, including monocytes/macrophages, DCs, and FDCs

Next, using the hNOG mice at 4 months after transplantation, we investigated lymphoid structure formation and the development of human monocytes, macrophages, DCs, and FDCs, which are very important factors not only for elicitation of immune responses against foreign antigens, but also for the spread of HIV-1 infection in a body.[22-24] Human CD14$^+$ monocytes were detected in PB, the spleen, and BM using flow cytometry (Figure 2A). During immunohistochemical analysis, human CD45$^+$ leukocytes gathered in a form of follicle-like structures (FLSs) at the end of the central artery in the spleen (Figure 2B). From a serial section of the same region (Figure 2B-G), these structures consisted mainly of human CD20$^+$ B cells (Figure 2C) admixed with a small number of human CD3$^+$ T cells (Figure 2D). Hardly any human FDCs positive for DRC-1 were detected (data not shown), whereas a

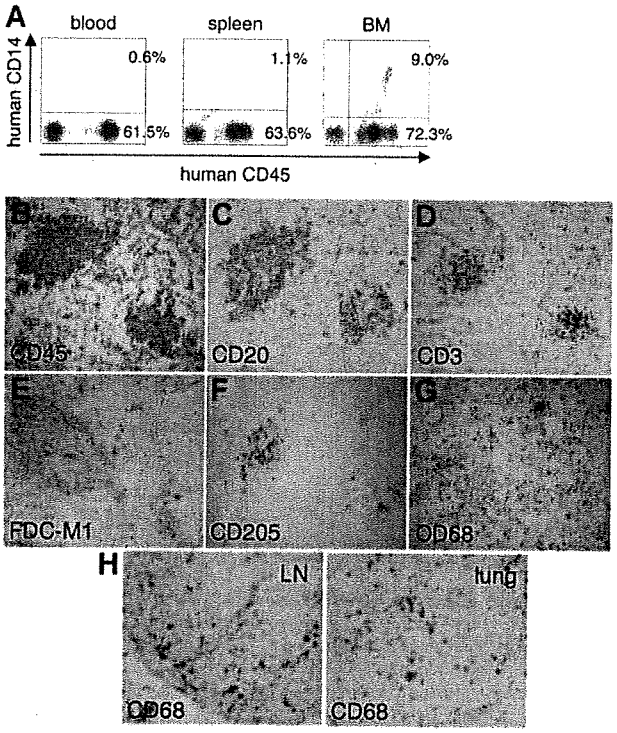


**Figure 2. Flow cytometric analysis and immunohistochemical analysis of the expression of myelomonocytic markers in hNOG mice 4 months after transplantation.** (A) Human CD14$^+$ monocytes/macrophages are recognized in peripheral blood, the spleen, and BM. (B-G) Immunohistochemical findings from serially sectioned spleen for the expressions of human CD45 (B), human CD20 (C), human CD3 (D), murine FDC (E), human CD205 (F), and human CD68 (G). (H) Human CD68$^+$ macrophages are also detected in the medulla of the LN and lung. Visualization was performed with BCIP (B-D, F-G), DAB (E), and AEC (H). Original magnification, ×100.

loose network of murine FDCs positive for FDC-M1 was recognized in the distal portion of the FLSs (Figure 2E). Human CD205$^+$ DCs were predominantly detected in a cluster form within the FLSs (Figure 2F), while human CD68$^+$ macrophages were scattered throughout the spleen (Figure 2G). Many human CD68$^+$ macrophages were also observed in various other organs, including the lymph nodes (LNs) and the lungs (Figure 2H).

### Expression of HIV-1 coreceptors on CD4$^+$ cells in various tissues

Since the development of lymphoid tissues was recognized in hNOG mice, we focused on the expressions of HIV-1 coreceptors CXCR4 and CCR5 on human CD4$^+$ cells in these tissues. CXCR4 antigen was expressed in 36.5% ± 4.2% (n = 4) of the CD4$^+$ cells in PB (Figure 3A) and 78.1% ± 17.1% (n = 5) in the spleen (Figure 3B). CCR5$^+$ cells were detected in 15.5% ± 1.8% (n = 4) of CD4$^+$ cells in PB and 28.6% ± 12.6% (n = 5) in the spleen (Figure 3A-B). In the thymus, CD4$^+$CD8$^+$ thymocytes existed in 82.9% ± 4.4% (n = 5) as well as small numbers of CD4$^+$CD8$^-$ cells (6.4% ± 2.4%; n = 5) and CD4$^-$CD8$^+$ cells (7.7% ± 3.0%; n = 5), with the CXCR4 antigen expressed in 50.1% ± 4.5% (n = 5) of CD4$^+$ cells, while, as with normal human thymocytes,[25] CCR5$^+$ cells were almost undetectable, with less than 1% (0.6% ± 0.1%; n = 5) (Figure 3C). Human CD3$^+$ T cells and CD14$^+$ monocytes in BM were detected only in 3.2% ± 2.1% and 5.8% ± 3.8%, respectively, while CD4$^+$ cells were recognized in 18.1% ± 6.5%, with many expressing both CXCR4 (75.0% ± 23.1%) and CCR5 (81.3% ± 6.6%; n = 5; Figure 3D). Thus, distributions of HIV-1 coreceptor–positive cells in these lymphoid tissues suggest that the hNOG mice allow for sufficient development of human cells to make the study of HIV-1 pathogenesis possible.

### Both R5- and X4-tropic HIVs efficiently infect and replicate in hNOG mice

In our preliminary study, using low and high doses of challenge virus, no viral infection was detected in any of the virus-inoculated hNOG mice at 7 days after infection, while some showed detectable plasma viral loads at 14 days (data not shown). Then, we prepared 16 hNOG mice that received transplants of stem cells and inoculated them with a high dose of R5-tropic HIV-1$_{JRCSF}$ (65 000 $TCID_{50}$) and X4-tropic SHIV-C2/1 (50 000 $TCID_{50}$) intravenously through the tail vein at 102 to 132 days after transplantation. Upon HIV-1$_{JRCSF}$ infection, viral copy numbers in plasma rose to a level of $1.6 \times 10^5$ to $5.8 \times 10^5$ copies/mL (n = 4) on day 33 and $2.0 \times 10^5$ to $4.7 \times 10^5$ copies/mL on day 43 (n = 4) (Figure 4A). Moreover, for SHIV-C2/1 infection, viral copy numbers in plasma were $1.6 \times 10^3$ to $3.2 \times 10^5$ copies/mL on day 18 (n = 4) and reached $5.4 \times 10^4$ to $1.1 \times 10^5$ copies/mL on day 42 (n = 4; Figure 4B). In these mice, no significant decline in the CD4/CD8 ratio was observed throughout entire period of follow-up for the R5-tropic virus infection, while CD4$^+$ cell decline was detected for the X4-tropic virus infection on day 42 after infection ($P$ = .044) but not on day 18 after infection (Figure 4C). Four mice that did not receive transplants of human stem cells showed no detectable levels of plasma viral load (less than 500 copies/mL) following HIV/SHIV inoculation (data not shown).

To confirm HIV infection, we used immunohistochemistry to detect the presence of the p24 antigen of the HIV-1 Gag protein in various tissues of mice showing viremia. p24$^+$ cells were clearly identified in the spleen, LN, and lungs (Figure 4D), which include macrophage-like cells.

### Different distributions of R5- and X4-tropic viruses in lymphoid tissues

A number of mice (14) were further analyzed for HIV-1 infection on days 126 to 146 after transplantation with a low dose (200 $TCID_{50}$) or a high dose (65 000 $TCID_{50}$) of R5-tropic HIV-1$_{JRCSF}$ and a low dose (180 $TCID_{50}$) or a high dose (20 000 $TCID_{50}$) of X4-tropic HIV-1$_{MNp}$. Consequently, 2 of the 4 mice given a low

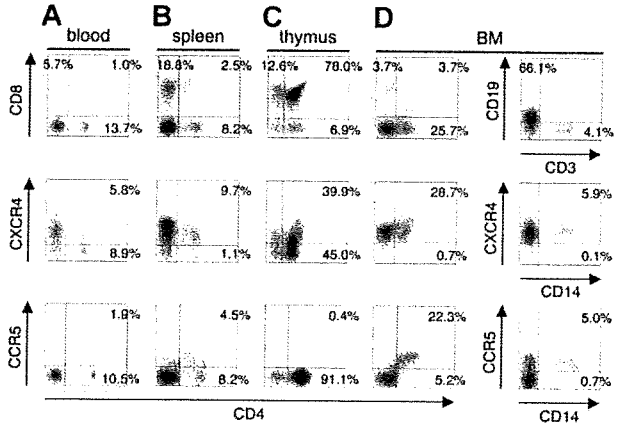


**Figure 3. Surface expression of HIV-1 coreceptors on CD4$^+$ cells in various organs of mice 4 months after transplantation.** A representative FACS profile of human CXCR4 and CCR5 on CD4$^+$ cells shows the existence of CXCR4$^+$CD4$^+$ and CCR5$^+$CD4$^+$ cells in blood (A), spleen (B), and BM (D), but no CCR5$^+$CD4$^+$ cells in the thymus (C). BM results show that many CD4$^+$ cells are neither CD3$^+$ T cells nor CD14$^+$ monocytes. A gate was set on the human CD45$^+$ population.

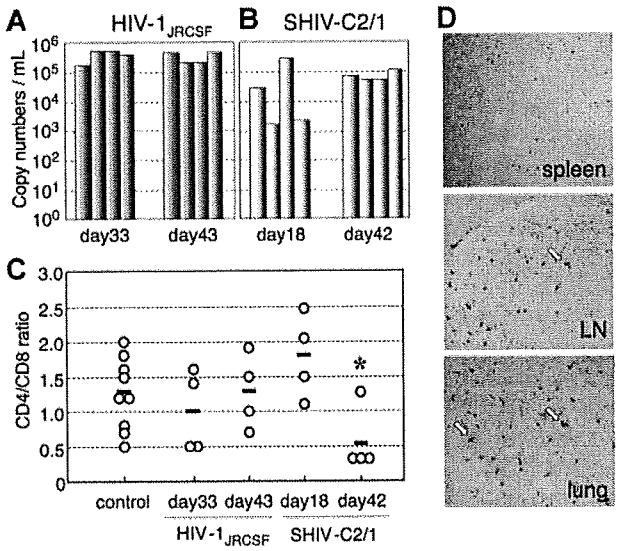


**Figure 4. The numbers of RNA viral copies in plasma, CD4+/CD8+ T-cell ratios in the spleen, and p24 detection in the immunohistochemistry of HIV/SHIV-infected mice.** (A) Viral copy numbers of 8 mice inoculated with a high infectious dose of HIV-$1_{JRCSF}$ (65 000 $TCID_{50}$) and killed on days 33 and 43 after inoculation. (B) Viral copy numbers of 8 mice inoculated with a high infectious dose of SHIV-C2/1 (50 000 $TCID_{50}$) and killed on days 18 and 42 after inoculation. Note that all the mice showed high levels of viremia that lasted more than 40 days after inoculation. (C) CD4/CD8 cell ratios in the spleens of 16 infected mice and 9 uninfected control mice. Control mice were not inoculated with HIV/SHIV and were killed on days 105 to 166 after stem cell transplantation. There was no significant rapid loss of $CD4^+$ cells in HIV-$1_{JRCSF}$–infected mice, while a decline of the CD4/CD8 ratio was detected in SHIV-C2/1–infected mice on day 42 after infection compared with uninfected control mice (*$P < .05$). The short bars indicate the means of each group. (D) $P24^+$ cells are clearly observed in the spleen, LNs, and lungs. Arrow indicates p24 positive for macrophage-like cells. Original magnification, ×100.

dose of HIV-$1_{JRCSF}$ and 2 of the 3 mice given a low dose of HIV-$1_{MNp}$ were successfully infected (Table 1), suggesting that each dose represents an approximately 50% infectious dose of HIV for hNOG mice. High HIV-DNA copy numbers were mainly detected in the spleen and BM of the HIV-$1_{JRCSF}$ –infected mice, and in the thymus and spleen of the HIV-$1_{MNp}$–infected mice, while their BM showed lower copy numbers (Table 1).

### Generation of HIV-specific antibodies in hNOG mice at a high multiplicity of infection

We then tested for generation of human antibodies against HIV-1 from these 14 mice by HIV antigen-specific ELISA. The sera of mice no. 136-3 and no. 157-3 infected with HIV-$1_{JRCSF}$ and HIV-$1_{MNp}$, respectively, showed significant levels of human antibodies specific for HIV-$1_{IIIB}$-Env gp120 (Figure 5A), HIV-$1_{MN}$-Env gp120 (Figure 5B), and HIV-$1_{IIIB}$-Gag p24 (Figure 5C). In addition, no. 157-4 sera from an HIV-$1_{MNp}$–infected animal was also weakly positive for their Env and Gag antigens. These animals showed intense plasma viral loads and enhanced proviral DNA copies in the spleen, BM, and thymus (Table 1), suggesting that hNOG mice inoculated with high doses of HIV and showing high rates of viral infection develop HIV-1–specific humoral immune responses that are analogous to those seen in human anti-HIV B-cell responses.

## Discussion

Current small-animal models fall short of accurately mirroring human HIV-1 infection and thus have limited usefulness in analyzing the natural course of its progression to the disease state and in developing antiviral countermeasures. Although successful HIV-1 infections in immunodeficiency mice humanized with PBMCs have been reported,[12,13,21] transplanted human cells are soon depleted and do not elicit virus-specific immune responses, shedding little light on pathogenesis and vaccine development. By using NOG mice that received hematopoietic stem cell transplants showing high rates of viral infection, we demonstrated HIV-specific antibody responses and viral infection parameters, including the following: (1) similar levels of susceptibility to both R5- and X4-tropic HIV-1; (2) high levels of viremia stably observed over 40 days; (3) immunohistochemical detection of infected cells in various organs; and (4) a distinct tissue distribution for R5- versus X4-tropic HIV-1s.

Among $CD4^+$ T cells, CXCR4 antigen is primarily expressed on naive and CCR5 on activated or memory cells.[26] hu-PBL-SCID mice become susceptible to R5-tropic HIV-1 strains,[27] since T cells

**Table 1. Comparison of viral RNA copies in plasma and HIV-DNA copies in the spleen, BM, and thymus from hNOG mice receiving low- and high-dose viral inoculations**

| Mouse ID no. | HIV strain | $TCID_{50}$ | Time after inoculation, d | RNA viral copies/mL | CD4/CD8 ratio | HIV-DNA copies/$10^6$ human cells | | |
|---|---|---|---|---|---|---|---|---|
| | | | | | | Spleen | BM | Thymus |
| **Low-dose viral inoculation group** | | | | | | | | |
| 113-1 | HIV-$1_{JRCSF}$ | 200 | 18 | 6 240 | 1.8 | 34 177 | 11 785 | 3 495 |
| 112-2 | HIV-$1_{JRCSF}$ | 200 | 18 | <500 | 1.2 | < 100 | < 100 | < 100 |
| 113-2 | HIV-$1_{JRCSF}$ | 200 | 40 | 6 177 | 1.6 | 25 855 | 27 920 | 3 473 |
| 112-3 | HIV-$1_{JRCSF}$ | 200 | 40 | <500 | 0.9 | < 100 | < 100 | <100 |
| 112-4 | HIV-$1_{MNp}$ | 180 | 18 | 72 477 | 1.3 | 18 873 | 100 | ND |
| 113-4 | HIV-$1_{MNp}$ | 180 | 40 | 70 667 | 0.3 | 4 947 | 653 | 32 163 |
| 112-1 | HIV-$1_{MNp}$ | 180 | 40 | <500 | 0.9 | < 100 | < 100 | < 100 |
| **High-dose viral inoculation group** | | | | | | | | |
| 136-3 | HIV-$1_{JRCSF}$ | 65 000 | 25 | 252 381 | 0.8 | 958 871 | 1 797 600 | 232 155 |
| 136-2 | HIV-$1_{JRCSF}$ | 65 000 | 29 | 50 167 | 0.7 | 41 172 | 54 521 | 8 600 |
| 141-1 | HIV-$1_{JRCSF}$ | 65 000 | 30 | 67 667 | 2.2 | 27 735 | 52 430 | 429 |
| 161-3 | HIV-$1_{JRCSF}$ | 65 000 | 30 | 13 847 | 0.9 | 104 466 | 14 653 | 111 080 |
| 157-3 | HIV-$1_{MNp}$ | 20 000 | 31 | 1 253 925 | 0.5 | 41 053 | 56 802 | 976 556 |
| 157-4 | HIV-$1_{MNp}$ | 20 000 | 31 | 147 973 | 0.6 | 3 634 | 262 | 40 796 |
| 161-6 | HIV-$1_{MNp}$ | 20 000 | 31 | 108 073 | 1.7 | 4 991 | < 100 | 3 673 |

Seven mice inoculated with a low infectious dose of HIV-$1_{JRCSF}$ (200 $TCID_{50}$) or HIV-$1_{MNp}$ (180 $TCID_{50}$), and 7 mice receiving a high infectious dose of HIV-$1_{JRCSF}$ (65 000 $TCID_{50}$) or HIV-$1_{MNp}$ (20 000 $TCID_{50}$) were listed.

ND indicates not done.

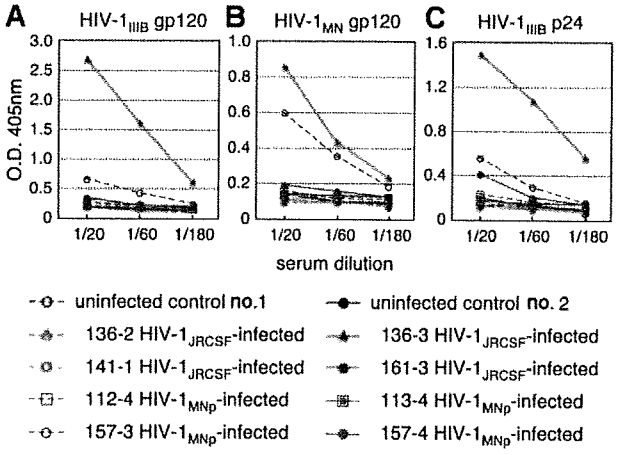


**Figure 5. Detection of anti–HIV-1 antibodies from the plasma of HIV-1–infected mice.** An ELISA assay was conducted by using plasma from 14 mice inoculated with either HIV-$1_{JRCSF}$ or HIV-$1_{MNp}$, and from 2 uninfected control mice. Representatives (n = 8) of the 14 HIV-1–inoculated mice, and the 2 uninfected mice, are shown in the panels. Measurements of specific human antibodies for HIV-$1_{IIIB}$ gp120 (A), HIV-$1_{MN}$ gp120 (B), and HIV-$1_{IIIB}$ p24 antigens (C) were shown. Results are expressed as the means from triplicate assays in 3 different experiments.

are initially activated in the xenogenic environment and then become anergic.[14] In contrast, SCID-hu (Thy/Liv) mice are more susceptible to X4 than to R5 strains[6] because HIV-1 infection is restricted mainly to the engrafted thymus that is primarily comprised of immature T cells, suggesting that this model may not be practical overt HIV infection. Our study represents the first attempt to infect NOG mice that received transplants of human hematopoietic stem cells with HIV-1. Very similar infection rates were seen for both R5 and X4 strains in the mouse model. Flow cytometry revealed both $CXCR4^+CD4^+$ and $CCR5^+CD4^+$ cells in PB, the spleen, and BM, but only CXCR4 on thymic $CD4^+$ T cells. It also showed the scattering of human macrophages, known to be susceptible to R5-tropic HIV-1 strains[28,29] and the source of HIV-1,[23,30-32] throughout various organs. $p24^+$ macrophage-like cells were detected in these organs after R5-tropic HIV-$1_{JRCSF}$ infection. These data may help explain the susceptibility of hNOG mice to both R5- and X4-tropic HIV strains and also shed light on the active replenishment of these target cells in mice.

SCID mouse systems have been actively used in the evaluation of anti–HIV-1 drugs.[9,11,21] In most cases, HIV-1 detection levels reach a peak within a month after inoculation and level off, accompanied by $CD4^+$ T-cell depletion.[3,12,13] Although suitable for short-term experiments, it is also true that these models require large numbers of mice because of large variations in infection efficiency. In contrast, very stable infections were noted in our hNOG mice that were inoculated with a high dose of HIVs. They did not show rapid CD4/CD8 decrease in spite of high levels of viremia persisting for more than 40 days. Efficient hematopoiesis and thymopoiesis of human cells probably compensated for the loss of $CD4^+$ T cells, allowing for persistent infection. This capacity of the hNOG mouse system makes it attractive as a model for the long-term evaluation of anti–HIV-1 drugs. In addition to destroying mature blood cells, altered hematopoiesis in BM and the thymus has also been reported to be responsible for immunodeficiency in patients with AIDS.[33,34] To study hematopoietic abnormalities in HIV-1 infection, both SCID-hu (Thy/Liv) mice[8,35,36] and SIV- or SHIV-infected macaque models[20,37-39] have been used. The current hNOG mouse system, in which human cells are efficiently reproduced from stem cells and then settled into hematopoietic organs, offers a promising model for the study of events that occur after infection not only with R5-tropic HIV-1 but also with X4-tropic HIV-1. Indeed, the BM of hNOG mice infected with R5-tropic HIV-1 exhibited exceptionally elevated levels of HIV-DNA copies. On the other hand, the thymus of X4-tropic HIV-$1_{MNp}$–infected hNOG mice yielded large numbers of HIV-DNA copies, which seemed to correlate with the predominant expression of CXCR4 on the thymocytes. Thus, further observation is essential to address whether AIDS symptoms such as considerable $CD4^+$ T-cell depletion and hematopoietic abnormalities eventually occur in these mice.

It is noteworthy that human antibodies against both HIV-1 Env gp120 and Gag p24 antigens were detected in mice no. 136-3, no. 157-3, and no. 157-4 after exposure to high titers of HIV-1, suggesting that hNOG mice have the ability to respond to HIV-1 antigens. This encourages us to develop antibody-based HIV vaccine candidates, although additional modifications are required for the stable induction of immune responses. Importantly, since the seroconverted mice showed high viremia and high numbers of proviral DNA copies in the spleen, BM, and thymus, abundant viral production may stimulate human B-cell responses against HIV-1 and generate specific antibodies. These mice showed little or no detectable human IgG against HIV-1, as determined by Western blot analysis (data not shown), suggesting that very low levels of class-switching occurred in these mice, though further study is required.

In addition to the humoral immune responses, the induction of primary T-cell responses is critical for the study of HIV-specific immune responses and pathogenesis, as well as for vaccine development. Although we did not demonstrate the T-cell ability to respond to virus antigens, human T cells from the spleen proliferated when stimulated with anti–human CD3 antibodies (data not shown), indicating that the human T cells in the NOG mice that received transplants of hematopoietic stem cells are capable of responding to T-cell receptor–mediated signals and are expected to be able to elicit primary antigen-specific immune responses against foreign antigens. To address whether the specific T-cell responses may be induced will be one of the important studies.

In conclusion, the NOG mice that received transplants of human hematopoietic stem cells successfully achieved systemic and persistent infection with both R5-tropic and X4-tropic HIV-1, and generated humoral immune responses against HIV-1. These capacities of the hNOG mouse model may be very attractive for the study of HIV pathogenesis and humoral immune responses induced by HIV vaccine candidates.

## Acknowledgments

We thank Yuetsu Tanaka of the University of Ryukyus, Tetsutaro Sata of NIID, and Shuzo Matsushita of Kumamoto University for their kind provision of mAbs to HIV-1, as well as Yukoku Tamaoka of Saiseikai Central Hospital, Toshio Akashi of Kumakiri Obstetric and Gynecologic Clinic, and Hideo Mugishima of Nihon University School of Medicine for their provision of umbilical cord blood. We also would like to express our gratitude to Ken Watanabe and Hideko Ogata of Tokyo Medical and Dental University for their skillful technical support.

This work was supported by grants from Research on Health Sciences focusing on Drug Innovation, the Japan Health Sciences Foundation.

## Authorship

Contributions: S.W., K.T., N.S., M.H., and N.Y. designed the study; S.W., K.T., S.O., S.H., M.Y., Y.S., M.Z.D., and Z.Y. carried out the research; M.I. contributed live mice; S.W., K.T., and T.M. analyzed the data; N.S., M.H., and N.Y. controlled the data; S.W. wrote the paper; and all authors checked the final version of the manuscript.

Conflict-of-interest statement: The authors declare no competing financial interests.

Correspondence: Naoki Yamamoto, AIDS Research Center, National Institute of Infectious Diseases, 1-23-1 Toyama, Shinjuku-ku, Tokyo 162-8640, Japan; e-mail: nyama@nih.go.jp; Mitsuo Honda, AIDS Research Center, National Institute of Infectious Diseases, 1-23-1 Toyama, Shinjuku-ku, Tokyo 162-8640, Japan; e-mail: mhonda@nih.go.jp; and Norio Shimizu, Department of Virology, Division of Medical Science, Medical Research Institute, Tokyo Medical and Dental University, 1-5-45 Yushima, Bunkyo-ku, Tokyo 113-8519, Japan; e-mail: nshivir@tmd.ac.jp.

## References

1. Letvin NL, Barouch DH, Montefiori DC. Prospects for vaccine protection against HIV-1 infection and AIDS. Annu Rev Immunol. 2002;20:73-99.
2. Namikawa R, Kaneshima H, Lieberman M, Weissman IL, McCune JM. Infection of the SCID-hu mouse by HIV-1. Science. 1988;242: 1684-1686.
3. Bonyhadi ML, Rabin L, Salimi S, et al. HIV induces thymus depletion in vivo. Nature. 1993; 363:728-732.
4. Aldrovandi GM, Feuer G, Gao L, et al. The SCID-hu mouse as a model for HIV-1 infection. Nature. 1993;363:732-736.
5. Su L, Kaneshima H, Bonyhadi M, et al. HIV-1-induced thymocyte depletion is associated with indirect cytopathogenicity and infection of progenitor cells in vivo. Immunity. 1995;2:25-36.
6. Kaneshima H, Su L, Bonyhadi ML, Connor RI, Ho DD, McCune JM. Rapid-high, syncytium-inducing isolates of human immunodeficiency virus type 1 induce cytopathicity in the human thymus of the SCID-hu mouse. J Virol. 1994;68:8188-8192.
7. Jenkins M, Hanley MB, Moreno MB, Wieder E, McCune JM. Human immunodeficiency virus-1 infection interrupts thymopoiesis and multilineage hematopoiesis in vivo. Blood. 1998;91:2672-2678.
8. Koka PS, Fraser JK, Bryson Y, et al. Human immunodeficiency virus inhibits multilineage hematopoiesis in vivo. J Virol. 1998;72:5121-5127.
9. Mosier DE, Gulizia RJ, Baird SM, Wilson DB, Spector DH, Spector SA. Human immunodeficiency virus infection of human-PBL-SCID mice. Science. 1991;251:791-794.
10. Torbett BE, Picchio G, Mosier DE. hu-PBL-SCID mice: a model for human immune function, AIDS, and lymphomagenesis. Immunol Rev. 1991;124: 139-164.
11. Ruxrungtham K, Boone E, Ford H Jr, Driscoll JS, Davey RT Jr, Lane HC. Potent activity of 2′-beta-fluoro-2′,3′-dideoxyadenosine against human immunodeficiency virus type 1 infection in hu-PBL-SCID mice. Antimicrob Agents Chemother. 1996;40:2369-2374.
12. Mosier DE, Gulizia RJ, MacIsaac PD, Torbett BE, Levy JA. Rapid loss of CD4+ T cells in human-PBL-SCID mice by noncytopathic HIV isolates. Science. 1993;260:689-692.
13. Koyanagi Y, Tanaka Y, Kira J, et al. Primary human immunodeficiency virus type 1 viremia and central nervous system invasion in a novel hu-PBL-immunodeficient mouse strain. J Virol. 1997; 71:2417-2424.
14. Tary-Lehmann M, Saxon A, Lehmann PV. The human immune system in hu-PBL-SCID mice. Immunol Today. 1995;16:529-533.
15. Ito M, Hiramatsu H, Kobayashi K, et al. NOD/SCID/gamma(c)(null) mouse: an excellent recipient mouse model for engraftment of human cells. Blood. 2002;100:3175-3182.
16. Yahata T, Ando K, Nakamura Y, et al. Functional human T lymphocyte development from cord blood CD34+ cells in nonobese diabetic/Shi-scid, IL-2 receptor gamma null mice. J Immunol. 2002; 169:204-209.
17. Hiramatsu H, Nishikomori R, Heike T, et al. Complete reconstitution of human lymphocytes from cord blood CD34+ cells using the NOD/SCID/gammacnull mice model. Blood. 2003;102:873-880.
18. Matsumura T, Kametani Y, Ando K, et al. Functional CD5+ B cells develop predominantly in the spleen of NOD/SCID/gammac(null) (NOG) mice transplanted either with human umbilical cord blood, bone marrow, or mobilized peripheral blood CD34+ cells. Exp Hematol. 2003;31:789-797.
19. Shinohara K, Sakai K, Ando S, et al. A highly pathogenic simian/human immunodeficiency virus with genetic changes in cynomolgus monkey. J Gen Virol. 1999;80:1231-1240.
20. Yamakami K, Honda M, Takei M, et al. Early bone marrow hematopoietic defect in simian/human immunodeficiency virus C2/1-infected macaques and relevance to advance of disease. J Virol. 2004;78:10906-10910.
21. Nakata H, Maeda K, Miyakawa T, et al. Potent anti-R5 human immunodeficiency virus type 1 effects of a CCR5 antagonist, AK602/ONO4128/GW873140, in a novel human peripheral blood mononuclear cell nonobese diabetic-SCID, interleukin-2 receptor gamma-chain-knocked-out AIDS mouse model. J Virol. 2005;79:2087-2096.
22. Heath SL, Tew JG, Tew JG, Szakal AK, Burton GF. Follicular dendritic cells and human immunodeficiency virus infectivity. Nature. 1995;377:740-744.
23. Orenstein JM, Fox C, Wahl SM. Macrophages as a source of HIV during opportunistic infections. Science. 1997;276:1857-1861.
24. van Kooyk Y, Geijtenbeek TB. A novel adhesion pathway that regulates dendritic cell trafficking and T cell interactions. Immunol Rev. 2002;186: 47-56.
25. Taylor JR Jr, Kimbrell KC, Scoggins R, Delaney M, Wu L, Camerini D. Expression and function of chemokine receptors on human thymocytes: implications for infection by human immunodeficiency virus type 1. J Virol. 2001;75:8752-8760.
26. Bleul CC, Wu L, Hoxie JA, Springer TA, Mackay CR. The HIV coreceptors CXCR4 and CCR5 are differentially expressed and regulated on human T lymphocytes. Proc Natl Acad Sci U S A. 1997; 94:1925-1930.
27. Fais S, Lapenta C, Santini SM, et al. Human immunodeficiency virus type 1 strains R5 and X4 induce different pathogenic effects in hu-PBL-SCID mice, depending on the state of activation/differentiation of human target cells at the time of primary infection. J Virol. 1999;73:6453-6459.
28. Gartner S, Markovits P, Markovitz DM, Kaplan MH, Gallo RC, Popovic M. The role of mononuclear phagocytes in HTLV-III/LAV infection. Science. 1986;233:215-219.
29. Koyanagi Y, Miles S, Mitsuyasu RT, Merrill JE, Vinters HV, Chen IS. Dual infection of the central nervous system by AIDS viruses with distinct cellular tropisms. Science. 1987;236:819-822.
30. Gendelman HE, Orenstein JM, Baca LM, et al. The macrophage in the persistence and pathogenesis of HIV infection. AIDS. 1989;3:475-495.
31. Embretson J, Zupancic M, Ribas JL, et al. Massive covert infection of helper T lymphocytes and macrophages by HIV during the incubation period of AIDS. Nature. 1993;362:359-362.
32. Igarashi T, Brown CR, Endo Y, et al. Macrophage are the principal reservoir and sustain high virus loads in rhesus macaques after the depletion of CD4+ T cells by a highly pathogenic simian immunodeficiency virus/HIV type 1 chimera (SHIV): implications for HIV-1 infections of humans. Proc Natl Acad Sci U S A. 2001;98:658-663.
33. Mir N, Costello C, Luckit J, Lindley R. HIV-disease and bone marrow changes: a study of 60 cases. Eur J Haematol. 1989;42:339-343.
34. Moses A, Nelson J, Bagby GC Jr. The influence of human immunodeficiency virus-1 on hematopoiesis. Blood. 1998;91:1479-1495.
35. Koka PS, Jamieson BD, Brooks DG, Zack JA. Human immunodeficiency virus type 1-induced hematopoietic inhibition is independent of productive infection of progenitor cells in vivo. J Virol. 1999;73:9089-9097.
36. Koka PS, Kitchen CM, Reddy ST. Targeting c-Mpl for revival of human immunodeficiency virus type 1-induced hematopoietic inhibition when CD34+ progenitor cells are re-engrafted into a fresh stromal microenvironment in vivo. J Virol. 2004;78: 11385-11392.
37. Hillyer CD, Lackey DA 3rd, Villinger F, Winton EF, McClure HM, Ansari AA. CD34+ and CFU-GM progenitors are significantly decreased in SIVsmm9 infected rhesus macaques with minimal evidence of direct viral infection by polymerase chain reaction. Am J Hematol. 1993;43:274-278.
38. Thiebot H, Louache F, Vaslin B, et al. Early and persistent bone marrow hematopoiesis defect in simian/human immunodeficiency virus-infected macaques despite efficient reduction of viremia by highly active antiretroviral therapy during primary infection. J Virol. 2001;75:11594-11602.
39. Thiebot H, Vaslin B, Derdouch S, et al. Impact of bone marrow hematopoiesis failure on T-cell generation during pathogenic simian immunodeficiency virus infection in macaques. Blood. 2005; 105:2403-2409.

THE JOURNAL OF BIOLOGICAL CHEMISTRY VOL. 282, NO. 50, pp. 36671–36681, December 14, 2007


# A Suppressive Role of the Prolyl Isomerase Pin1 in Cellular Apoptosis Mediated by the Death-associated Protein Daxx*

Received for publication, May 21, 2007, and in revised form, September 17, 2007 Published, JBC Papers in Press, October 15, 2007, DOI 10.1074/jbc.M704145200

**Akihide Ryo[‡1], Akiko Hirai[‡], Mayuko Nishi[‡], Yih-Cherng Liou[§2], Kilian Perrem[¶], Sheng-Cai Lin[‖], Hisashi Hirano[**], Sam W. Lee[‡‡], and Ichiro Aoki[‡]**

*From the [‡]Department of Pathology, Yokohama City University School of Medicine, 3-9 Fuku-ura, Kanazawa-ku, Yokohama 236-0004, Japan, the [§]Department of Biological Sciences, National University of Singapore, Singapore 117543, Singapore, the [¶]Molecular Oncology Laboratory, Department of Pathology, Royal College of Surgeons in Ireland, Smurfit Building, Beaumont Hospital, Dublin 9, Ireland, the [‖]Key Laboratory of the Ministry of Education for Cell Biology, School of Life Sciences, Xiamen University, Fujian 361005, Xiamen, China, the [**]International Graduate School of Arts and Sciences, Yokohama City University, Yokohama 230-0045, Japan, and the [‡‡]Cutaneous Biology Research Center, Massachusetts General Hospital and Harvard Medical School, Charlestown, Massachusetts 02129*

**The death-associated protein Daxx is a multifunctional factor that regulates a variety of cellular processes, including transcription and apoptosis. Several previous reports have indicated that Daxx is induced upon oxidative stress and is then subjected to phosphorylation-based functional modification. However, the precise molecular events underlying these phosphorylation events remain largely unknown. We report in our current study that the peptidyl-prolyl isomerase Pin1 is highly overexpressed in malignant human gliomas and inhibits Daxx-mediated cellular apoptosis. The targeted inhibition of Pin1 by small interfering RNA in A172 glioblastoma cells significantly enhances the apoptotic response induced by hydrogen peroxide or stimulatory Fas antibodies. This is in turn accompanied by the increased induction of Daxx and the activation of the apoptosis signal-regulating kinase 1/c-Jun N-terminal kinase pathway. Furthermore, Pin1 binds to the phosphorylated Ser[178]-Pro motif in the Daxx protein, and Pin1 overexpression results in the rapid degradation of Daxx via the ubiquitin-proteasome pathway. Moreover, a Daxx-S178A mutant, which cannot interact with Pin1, demonstrates higher proapoptotic activity and is refractory to Pin1-mediated antiapoptotic effects. We further found that the expression levels of Pin1 inversely correlate with the degree of Daxx nuclear accumulation in human glioblastoma tissues. These results together indicate that Pin1-mediated prolyl isomerization plays an important role in the negative regulation of Daxx and thereby inhibits the oxidative stress-induced cellular apoptotic response, particularly in malignant tumor cells where Pin1 is often overexpressed.**

Oncogenesis comprises a complex series of multistep and multifactorial processes that result in uncontrolled cell proliferation, cell transformation, and cell death (1). The resistance to apoptosis in malignant tumor cells is one of the most critical factors that directly contribute to tumor cell proliferation and expansion (2). Furthermore, this apoptotic evasion represents one of the true hallmarks of cancer and appears to be a vital component in chemotherapeutic and radiotherapeutic resistance that characterizes the aggressiveness of human malignant tumors (1).

The antiapoptotic characteristics of tumor cells are often derived from the improper regulation of proapoptotic signaling pathways by various external and internal stimuli (3). One of the pivotal signaling mechanisms that controls cellular apoptotic processes is the phosphorylation of proteins on serine or threonine residues preceding proline (Ser/Thr-Pro) (4, 5). The recent identification and characterization of the peptidyl-prolyl isomerase Pin1, which can recognize these phosphorylated moieties, has led to the elucidation of a number of novel postphosphorylation regulatory mechanisms (4). Pin1 catalyzes the cis-trans isomerization of phosphorylated Ser/Thr-Pro motifs within its specific target substrates (4, 5). Pin1-mediated prolyl isomerization has also now been shown to function in several signaling pathways during tumorigenesis, including Wnt/β-catenin and NF-κB (6, 7). Pin1 is further implicated in many pivotal oncogenic cellular events, such as cell proliferation, angiogenesis, and tumor metastasis (8). However, although some of the roles of Pin1 in several oncogenic signaling pathways have been addressed, there has been no direct evidence reported to date showing that Pin1 can inhibit cellular apoptosis in malignant tumor cells.

The death-associated protein Daxx was originally identified as a Fas-interacting protein that specifically binds to the death domain of Fas and then facilitates Fas-mediated apoptosis independently of FADD (9). Several lines of evidence presented in recent studies have indicated that Daxx plays a crucial role in the cellular apoptotic response induced by UV, oxidative stress, and glucose deprivation, in addition to its function during Fas-mediated apoptosis (10). Daxx has also been reported to localize at the promyelocytic leukemia nuclear bodies in nonapoptotic cells (11). Indeed, nuclear Daxx has been demonstrated to regulate transcription by acting as a transcriptional corepressor via its interaction with several transcription factors (12). Several additional studies have also addressed the potential cyto-

* This work was supported in part by a special fellow grant from the Leukemia and Lymphoma Society and by grants from the Ministry of Education, Culture, Sports, Science and Technology of Japan (to A. R.). The costs of publication of this article were defrayed in part by the payment of page charges. This article must therefore be hereby marked "*advertisement*" in accordance with 18 U.S.C. Section 1734 solely to indicate this fact.

[1] To whom correspondence should be addressed. Tel.: 81-45-787-2587; Fax: 81-45-786-0191; E-mail: aryo@yokohama-cu.ac.jp.

[2] Supported by grants from the National Science Foundation of China and the Biomedical Research Council of Singapore.

plasmic *versus* nuclear roles of Daxx toward the triggering of apoptotic pathways (13). Upon various stimuli, such as serum depletion or oxidative stress, Daxx is phosphorylated and retranslocated from the cytoplasm to the nucleus via the exportin-mediated nuclear transport system (14). Cytoplasmic Daxx can interact with apoptosis signal-regulating kinase 1 (ASK1)[3] and then activate the ASK1/c-Jun-N-terminal kinase (JNK) signaling pathway. In fact, Daxx-depleted cells have been shown to be resistant to cell death pathways induced by both UV irradiation and oxidative stress following impaired ASK1/JNK activation (13). Although the phosphorylation of Daxx has also been shown to regulate its subcellular localization and function following proapoptotic stimuli, it is not known whether its protein stability is regulated by phosphorylation or by other post-translational modifications.

The aim of our present study was to clarify the regulation of Daxx by phosphorylation-dependent prolyl isomerization mediated by Pin1. The importance of both the physical and functional interactions between Daxx and Pin1 during the induction of cell death pathways following exposure to oxidative stress was also investigated, and the involvement of the ASK1/JNK pathway was also evaluated. We find from the results of these analyses that the targeted inhibition of Pin1 in human glioblastoma A172 cells significantly sensitizes these cells to oxidative stress-induced apoptosis, suggesting that Pin1 can protect against the Daxx-mediated apoptotic response. We also find that Pin1 can bind Daxx via its phosphorylated $Ser^{178}$-Pro motif and facilitate its prompt degradation via the ubiquitin-proteasome pathway. This results in the inhibition of the proapoptotic functions of Daxx. Our present results have thus uncovered a novel molecular mechanism underlying the post-translational regulation of Daxx and demonstrate that Pin1 acts as a putative antiapoptotic molecule in malignant tumor cells.

## EXPERIMENTAL PROCEDURES

*Immunohistochemistry*—Human glioma tissue microarrays (US Biomax, Rockville, MD) were analyzed immunohistochemically using a Pin1 antibody as previously described (15). Briefly, paraffin-embedded tissue sections were deparaffinized and rehydrated. After microwave antigen retrieval in sodium citrate buffer, endogenous peroxidase activity was quenched by immersion in 0.3% $H_2O_2$. The sections were then treated with anti-Pin1 polyclonal antibodies (Santa Cruz Biotechnology, Santa Cruz, CA) at a 1:200 dilution overnight at 4 °C, after blocking with 5% normal goat serum for 30 min at room temperature. Biotinylated goat anti-rabbit immunoglobulin G (Vector Laboratories, Burlingame, CA) was then used as the secondary antibody at a 1:200 dilution for 30 min at room temperature. The sections were subsequently treated using a peroxidase-labeled Vectastain Elite ABC kit (Vector Laboratories), at a 1:200 dilution for 30 min at room temperature. Labeled antigen was visualized via a 3,3′-diaminobenzidine reaction, and each of the sections was counterstained with hematoxylin. The expression level of Pin1 was evaluated as described previously (15).

*Retroviral siRNA Infection*—A Pin1-specific siRNA retroviral vector was prepared as previously described (8). Target cell lines were treated with the indicated retrovirus and selected by continuous growth in puromycin (1.0–1.5 μg/ml) for 48 h to isolate stable clones.

*siRNA Oligonucleotides*—Human Daxx siRNA and scrambled control siRNA oligonucleotides were purchased from Santa Cruz Biotechnology. The final concentration of siRNA oligonucleotides was 200 nmol/liter, and these molecules were introduced into cells using Lipofectamine 2000 (Invitrogen) according to the manufacturer's instructions.

*Cell Culture and Transient Transfections*—A172, 293T, and HeLa cells were cultured in Dulbecco's modified Eagle's medium supplemented with 10% fetal bovine serum and 1% penicillin (100 mg/ml), streptomycin (50 μg/ml). Transient transfections were carried out using either Effectene Transfection Reagent (Qiagen) or HilyMax (DOJINDO, Kumamoto, Japan).

*Protein Degradation Assay*—Protein degradation assays were performed as described previously (6). Briefly, 293T cells were co-transfected with FLAG-Daxx and either wild-type Pin1 or empty vector, with GFP used as a transfection control. Cycloheximide (50 μg/ml) was added to the medium 24 h after transfection, and the cells were harvested at different time points. Total cell lysates in SDS sample buffer were boiled and then analyzed by immunoblotting with either anti-FLAG (Sigma) or anti-Pin1 (R&D System) or GFP (Invitrogen) antibodies.

*GST Pull-down, Immunoprecipitation, and Immunoblotting Analyses*—293T cells was lysed with GST pull-down buffer (50 mM HEPES (pH 7.4), 150 mM NaCl, 10% glycerol, 1% Triton X-100, 1.5 mM $MgCl_2$, 1 mM EGTA, 1 mM EDTA, 100 mM NaF, 1 mM $Na_3VO_4$, 1 mM dithiothreitol, 0.5 μg/ml leupeptin, 1.0 μg/ml pepstatin, 10 μM MG132, 10 μM MG115, and 0.2 mM phenylmethylsulfonyl fluoride) and incubated with 30 μl of glutathione-agarose beads containing either GST-Pin1 or GST at 4 °C for 2 h. The precipitated proteins were then washed three times with GST pull-down buffer and subjected to SDS-PAGE (7). For immunoprecipitation, cells were harvested 24 h after transfection and lysed with radioimmune precipitation buffer (20 mM Tris-HCl (pH 7.5), 150 mM NaCl, 2 mM EDTA, 1% Nonidet P-40, 1% sodium deoxycholate, 0.1% SDS, 1 mM $Na_3VO_4$, 50 mM NaF, 0.5 μg/ml leupeptin, 1.0 μg/ml pepstatin, 10 μM MG132, 10 μM MG115, and 0.2 mM phenylmethylsulfonyl fluoride). Cell lysates were then incubated for 1 h with protein A/G-Sepharose-nonimmunized IgG complexes. Supernatant fractions were recovered and immunoprecipitated with 5 μg of anti-FLAG or anti-Myc antibody and 30 μl of protein A/G-Sepharose. After washing three times with radioimmune precipitation buffer, pellets were analyzed on SDS-polyacrylamide gels and subjected to immunoblotting analysis. The antibodies used in this study were obtained from the following sources: mouse monoclonal anti-Daxx, mouse monoclonal anti-Fas (SH-11), and rabbit polyclonal anti-GFP antibodies (MBL International); rabbit polyclonal anti-phospho-ASK1 ($Ser^{83}$) and cleaved caspase-3 ($Asp^{175}$) antibodies (Cell Signal-

[3] The abbreviations used are: ASK1, apoptosis signal-regulating kinase 1; TUNEL, terminal deoxynucleotidyltransferase-mediated deoxyuridine triphosphate biotin nick end labeling; JNK, c-Jun N-terminal kinase; siRNA, small interfering RNA; GFP, green fluorescent protein; GST, glutathione *S*-transferase; PPIase, prolyl isomerase.

ing); mouse monoclonal anti-phospho-JNK (Thr(P)$^{183}$/Tyr(P)$^{185}$) antibody (BD Biosciences); rabbit polyclonal anti-Pin1 (H-123) and rabbit polyclonal anti-JNK (C-17) antibodies (Santa Cruz Biotechnology); anti-Pin1 monoclonal antibody (R & D Systems); rabbit polyclonal anti-cleaved poly(ADP-ribose) polymerase antibody (Abcam); mouse monoclonal anti-FLAG (M2); and anti-γ-tubulin antibodies (Sigma).

*Fluorescence Imaging*—HeLa cells on coverslips were co-transfected with pDs-Red-Daxx and pIRES-puro-GFP-Pin1 using HilyMax (DOJINDO), according to the manufacturer's instructions. 24 h after transfection, the cells were fixed with 3% formaldehyde and treated with phosphate-buffered saline and were then stained with 4′, 6-diamidino-2-phenylindole. After washing with phosphate-buffered saline, slides were visualized under a confocal laser microscope (Olympus, Tokyo, Japan) as described previously (16).

*Apoptosis Analysis*—Apoptotic cells were detected by the *in situ* TUNEL method using a DeadEnd Colorimetric TUNEL system (Promega), according to the manufacturer's protocol. Cells with apoptotic nuclei were detected by Hoechst 33258 staining with fluorescent microscopy as described previously (17). Cell viability was investigated with a trypan blue dye exclusion assay using 0.4% trypan blue dye (Sigma). The data were expressed as the mean ± S.D. from triplicate independent experiments.

*In Vitro Kinase Assay*—For the measurement of JNK1 activity *in vitro*, A172 cells were lysed in buffer containing 25 mM HEPES (pH 7.4), 150 mM NaCl, 20 mM β-glycerophosphate, 2 mM EDTA, 2 mM EGTA, 50 mM NaF, 1 mM sodium orthovanadate, 1% Triton X-100, and proteinase inhibitor mixture, as described previously (18). The lysates were then clarified by centrifugation and immunoprecipitated with the anti-JNK antibody C-17 (Santa Cruz Biotechnology) for 2 h. The immune complexes were recovered with protein A-Sepharose beads and washed twice with the above lysis buffer and twice with kinase buffer (25 mM HEPES (pH 7.4), 20 mM $MgCl_2$, 20 mM β-glycerophosphate, 0.5 mM EGTA, 0.5 mM NaF, 0.5 mM sodium orthovanadate). The immune complexes on the Sepharose beads were used in kinase assays with GST-c-Jun. The reaction was initiated by adding 30 μl of kinase reaction mixture (kinase buffer plus 5 μCi of [γ-$^{32}$P]ATP, 20 μM unlabeled ATP, 1 mM dithiothreitol, and 1 μg of a substrate). After 20 min of incubation at 30 °C, the reactions were terminated by the addition of 10 μl of 5× SDS-PAGE loading buffer. Samples were resolved by SDS-PAGE and visualized by autoradiography.

## RESULTS

*Pin1 Is Highly Expressed in Human Glioma*—It has been previously reported that Pin1 is highly overexpressed in various human malignancies, including breast and prostate cancers, and plays a crucial role in oncogenesis (4, 5). Since the relevance of Pin1 in the tumorigenesis of human glioma has not been well characterized, we investigated the correlation of Pin1 expression with the malignant properties of human gliomas. To this end, we first performed immunohistochemical analysis of a human glioma tissue panel, including normal brain tissue controls ($n = 9$), low grade astrocytomas (grade 2; $n = 24$), anaplastic astrocytomas (grade 3; $n = 45$), and glioblastomas (grade 4; $n = 28$), all classified according to World Health Organization

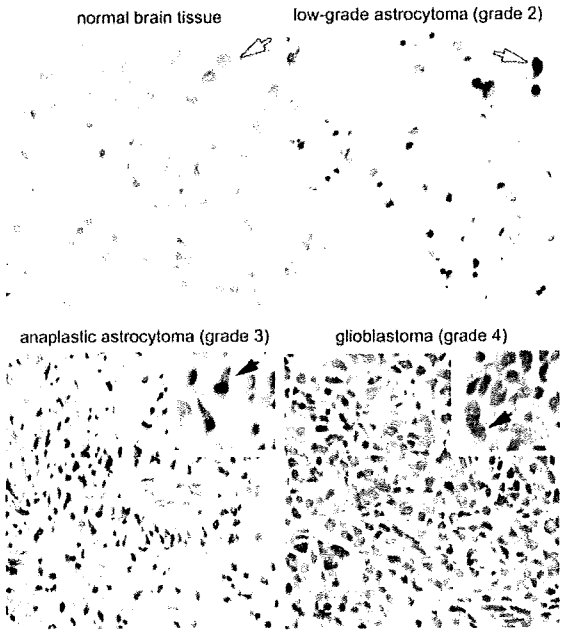


B

| | Pin1 expression | | | |
|---|---|---|---|---|
| | Low level | High level | Very high level | Total |
| Normal brain | 9(100%) | 0(0%) | 0(0%) | 9(100%) |
| Grade2 | 4(16.7%) | 13(54.2%) | 7(29.2%) | 24(100%) |
| Grade3 | 3(6.7%) | 20(44.4%) | 22(35.7%) | 45(100%) |
| Grade4 | 3(10.7%) | 15(53.6%) | 10(35.7%) | 28(100%) |
| Total | 19(17.9%) | 48(45.3%) | 39(36.8%) | 106(100%) |

FIGURE 1. **Pin1 is overexpressed in human glioma tissues.** *A*, tissues, including normal brain, a low grade astrocytoma (grade 2), an anaplastic astrocytoma (grade 3), and a glioblastoma (grade 4), were immunostained with anti-Pin1 antibodies. Nuclei were further stained with hematoxylin. Pin1 signals in nuclei only and in both the nuclei and cytoplasm are indicated by the *white* and *black arrows*, respectively. *B*, the ratio of cells with low, high, or very high Pin1 expression levels was scored for each of the glioma tissues in a panel of different grades and also in normal brain. A significant correlation between Pin1 expression levels and glioma grades was confirmed using a Spearman rank test ($p < 0.01$).

criteria. We found that Pin1 expression was significantly enhanced in glioma tissues compared with normal brain (Fig. 1*A*). Interestingly, Pin1 expression was found to be confined to the nuclei in both normal brain tissue and low grade astrocytoma at relatively low expression levels but exhibited enhanced expression in both the cytoplasm and nuclei of anaplastic astrocytoma and glioblastoma (Fig. 1*A*), as previously found also in other malignant tumors (15, 19). These immunohistochemical analyses indicate that the higher expression of Pin1 correlates with a more highly malignant glioma (Fig. 1*B*). Our results thus suggest a potential role for Pin1 in the development of these tumors.

*Loss of Pin1 Function Sensitizes Human Glioblastoma Cells to Oxidative Stress-induced Cell Death*—Our immunohistochemical analysis suggested that high levels of Pin1 expression in human gliomas could contribute to the acquisition of some of the malignant characteristics of these tumors. It has been reported that high grade gliomas are resistant to cellular apoptosis and that this could be important for tumor cell proliferation and drug resistance (20). To investigate whether Pin1 contributes to apoptotic resistance in glioma cells, we attempted to create stable human glioma cell lines in which Pin1 is constitutively suppressed.

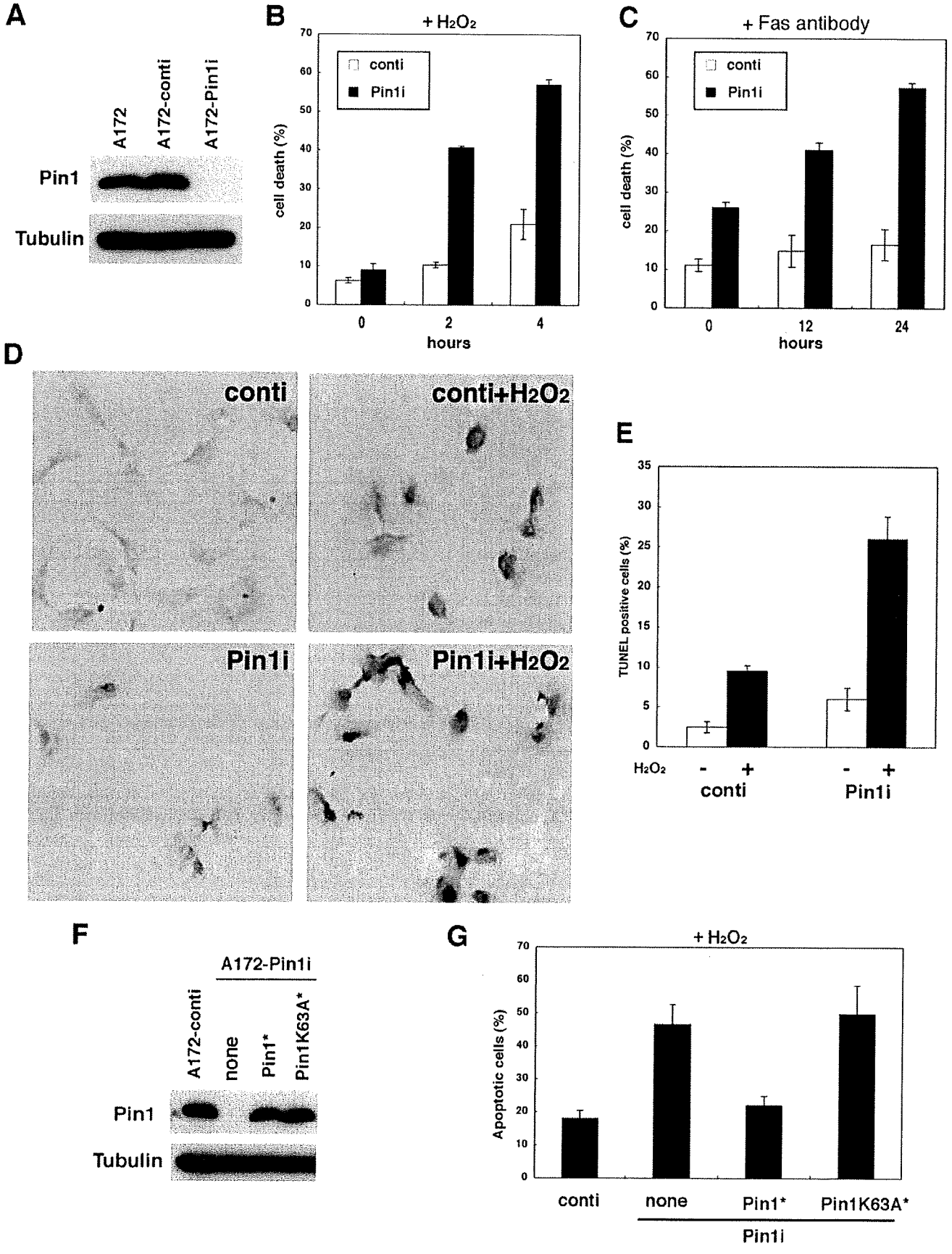

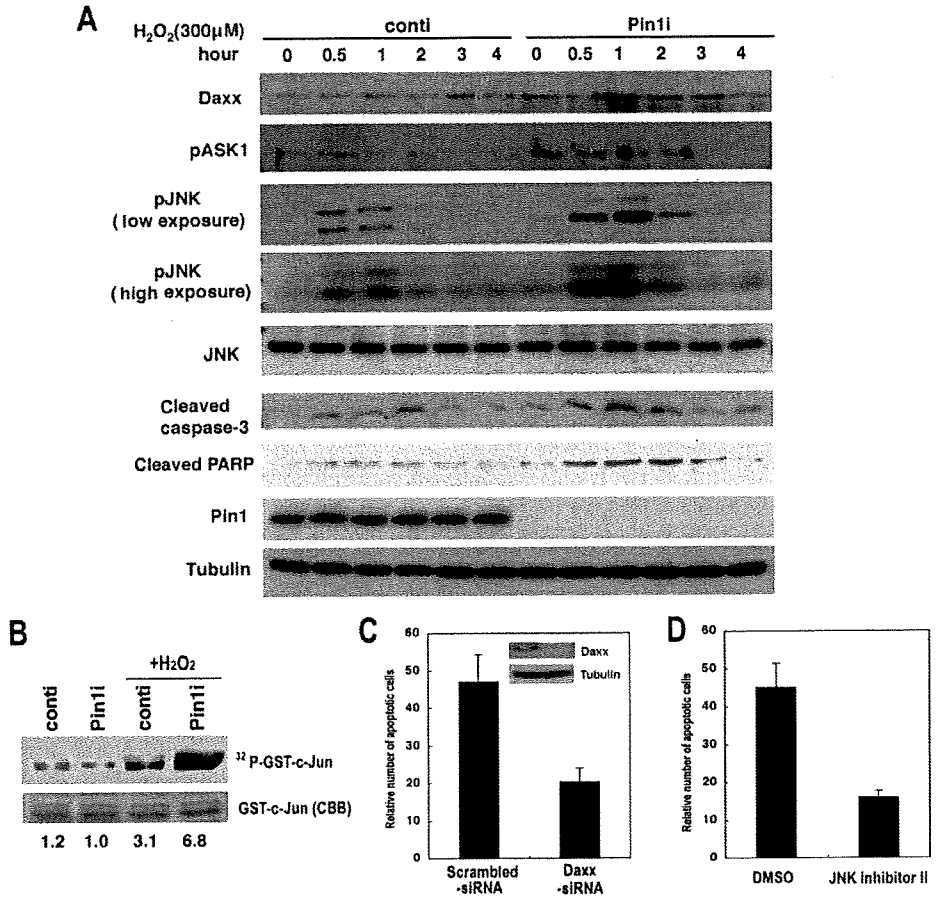


FIGURE 3. **The stable suppression of Pin1 enhances $H_2O_2$-induced Daxx expression and ASK1/JNK activation under conditions of oxidative stress.** *A*, A172 stable cells were treated with $H_2O_2$ (300 μM) and harvested at the indicated time points followed by immunoblotting with the indicated antibodies. *B*, A172 stable cells were untreated or treated with $H_2O_2$ (300 μM). After 3 h, cells were harvested and subjected to immunoprecipitation with anti-JNK1 antibody followed by *in vitro* kinase assay using GST-c-Jun as a substrate. *Numbers below the blots* indicate band intensity of $^{32}$P-labeled c-Jun quantitated by a PhosphorImager. *CBB*, Coomassie Brilliant Blue stain. *C*, A172-Pin1-siRNA (Pin1i) stable cells were transfected with either nonspecific (*scrambled*) or Daxx-targeted siRNA oligonucleotides. At 36 h after transfection, the cells were treated with $H_2O_2$ (300 μM) for 4 h and stained with Hoechst 33258 dye. Relative apoptotic cell numbers were scored out of 200 cells. *Inset*, immunoblotting with the indicated antibodies. *D*, A172-Pin1-siRNA (Pin1i) stable cells were pretreated with either JNK inhibitor II (20 μM) or $Me_2SO$ for 1 h and then exposed to $H_2O_2$ (300 μM) for another 4 h. The relative numbers of apoptotic cell were scored as in *C*. *DMSO*, $Me_2SO$.

To this end, we employed a representative human glioblastoma cell line, A172, since these cells have been reported to show antiapoptotic properties against oxidative stress stimuli and anti-tumor drugs (21). The retrovirus-mediated siRNA targeting of Pin1 in A172 cells (A172-Pin1i) was found to cause a marked knockdown of Pin1 expression (<95%), whereas the control siRNA expressing cells (A172-conti) showed Pin1 expression levels that were similar to the noninfected cells (Fig. 2*A*). We next treated these stable cell lines with either hydrogen peroxide ($H_2O_2$) or anti-Fas stimulatory antibodies to induce cellular apoptosis. We found that Pin1 depletion by siRNA significantly enhances the rate of cell death caused by both of these stimuli by ~3-fold compared with the control siRNA-expressing cells (Fig. 2, *B* and *C*). Consistent with these results, the A172-Pin1i cells exhibit a higher rate of TUNEL staining compared with A172-conti cells when treated with $H_2O_2$ (Fig. 2, *D* and *E*). Furthermore, the forced expression of wild-type Pin1, but not its peptidyl-prolyl isomerase mutant (K63A), which was not subject to knockdown by siRNA, reverted the apoptotic response in cells harboring Pin1 siRNA molecules to control levels (Fig. 2, *F* and *G*). These results verify that there is a specific role of endogenous Pin1 in the suppression of $H_2O_2$- or Fas-induced cellular apoptosis and suggest that the targeted inhibition of Pin1 in glioma cells causes an increased susceptibility to cellular apoptosis induced by oxidative stress.

*The Suppression of Pin1 Enhances Daxx Induction and Subsequent ASK1/JNK Activation toward Oxidative Stress-induced Cellular Apoptosis*—Our initial analysis indicated that the specific depletion of Pin1 enhances the apoptotic response to oxidative stress in human glioma cells. To delineate the molecular events underlying this phenomenon, we performed immunoblotting analysis to monitor the activity of the intracellular signaling pathways related to oxidative stress-induced cellular apoptosis. Since it has been reported that the activation of the Daxx-ASK1-JNK pathway is a critical event in the induction of cellular apoptosis by $H_2O_2$ (3), we evaluated the components of this pathway in our current experiments.

FIGURE 2. **The loss of Pin1 function sensitizes human glioblastoma cells to oxidative stress-induced cellular apoptosis.** *A*, stable suppression of Pin1 by retrovirus-mediated siRNA in A172 glioblastoma cells determined by immunoblotting analysis. Lysates from cells that were mock-infected or retrovirally infected with control siRNA (*conti*) or Pin1-specific siRNA (*Pin1i*) were immunoblotted with either anti-Pin1 or anti-γ-tubulin antibodies. *B* and *C*, the stable siRNA cell lines described in *A* were treated with either $H_2O_2$ (300 μM) (*B*) or stimulatory Fas antibodies (100 ng/ml) (C). At the indicated time points following these treatments, viable cell numbers were counted using trypan blue dye exclusion (mean ± S.D.). *D* and *E*, A172 stable cell lines treated with $H_2O_2$ (300 μM) were subjected to TUNEL staining. TUNEL-positive cells were visualized by staining with diaminobenzene (*DAB; brown*). Cells were also counterstained with 1% methyl green (*green*). TUNEL-positive cells were scored out of >200 cells from three independent experiments. *F* and *G*, A172-Pin1i cells were transfected with siRNA-resistant wild type Pin1 (*Pin1**) or a PPIase domain mutant Pin1-K63A (*Pin1-K63A**) and co-transfected with GFP as a transfection control. The expression of these Pin1 constructs was initially confirmed by immunoblot analysis with anti-Pin1 antibody (*F*). After 24 h, cells were seeded onto glass coverslips and treated with $H_2O_2$ (300 μM) for another 4 h. Cells were then fixed and immunostained with anti-cleaved caspase-3 antibody. The ratios of cleaved caspase-3-positive cells to GFP-positive cells were calculated from three independent experiments (mean ± S.D.) (*G*).

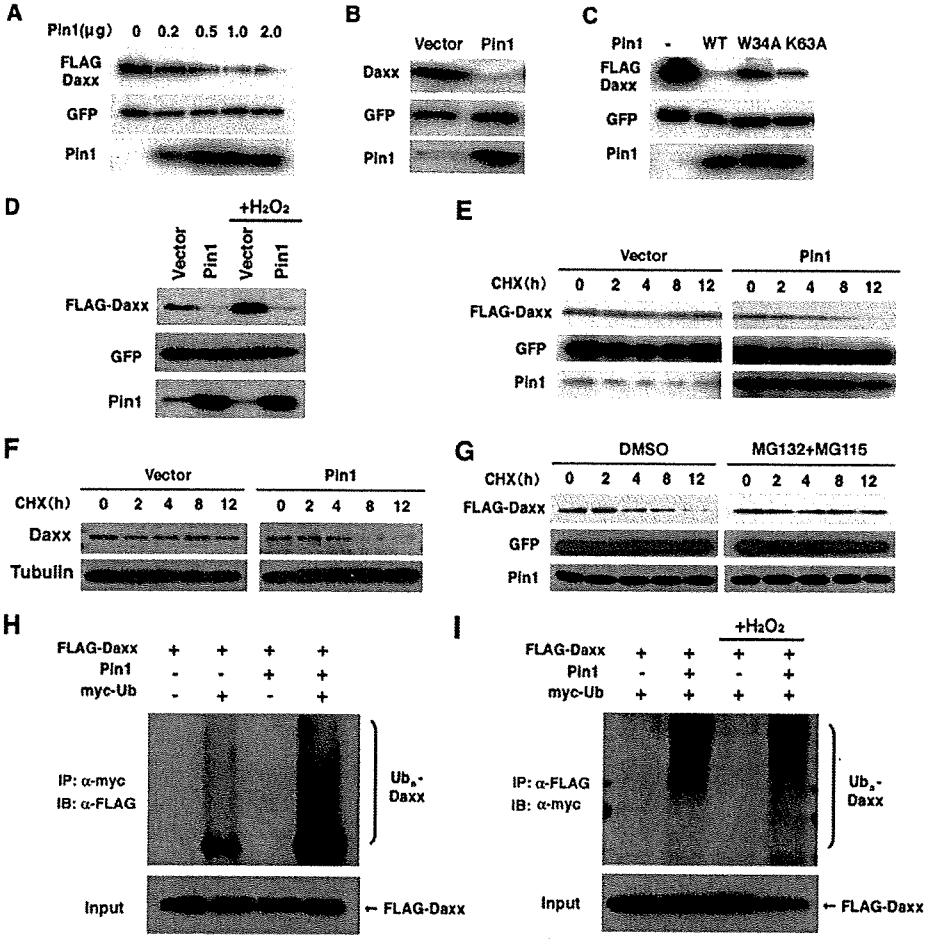


FIGURE 4. **Pin1 expression facilitates the degradation of Daxx via the ubiquitin-proteasome pathway.** *A*, 293T cells were co-transfected with FLAG-Daxx, GFP, or different amounts of Pin1 expression plasmids. After 24 h, the cells were harvested and subjected to immunoblotting analysis with either anti-FLAG or anti-GFP antibodies. *B*, 293T cells were transfected with either wild-type Pin1 or empty vector. After 24 h, the cells were subjected to immunoblotting with an anti-Daxx antibody to monitor the endogenous Daxx levels. *C*, 293T cells were transfected with FLAG-Daxx and co-transfected with either wild-type Pin1 (*WT*) or its W34A (WW domain) or K63A (PPIase domain) mutants. After 24 h, the cells were subjected to immunoblotting as indicated. *D*, 293T cells were co-transfected with FLAG-Daxx and GFP and co-transfected with either wild-type Pin1 or empty vector. After 24 h, the cells were treated with $H_2O_2$ for 3 h and then subjected to immunoblotting as indicated. *E*, 293T cells were co-transfected with the indicated vectors, treated with cycloheximide (*CHX*) after 24 h, and harvested at the indicated time points. This was followed by immunoblotting analysis with either anti-FLAG or anti-GFP antibodies. *F*, 293T cells were transfected with either Pin1 or control vector subjected to a cycloheximide assay as shown in *E*. Cells were harvested at the indicated time points followed by immunoblotting analysis. *G*, 293T cells were subjected to a cycloheximide assay, as shown in *E*, in the presence or absence of the proteasome inhibitors MG132 and MG115 (10 μM each). *H*, 293T cells were co-transfected with the indicated vectors and cotreated with the proteasome inhibitors MG132 and MG115 after 24 h. After a further 12 h, the cell lysates were subjected to immunoprecipitation (*IP*) analysis with anti-Myc antibodies followed by immunoblotting (*IB*) with anti-FLAG antibodies. $Ub_n$, polyubiquitinated. *I*, 293T cells were co-transfected with the indicated vectors. After 24 h following transfection, cells were treated with the proteasome inhibitor MG132 and MG115 (10 μM each) with or without $H_2O_2$ for 5 h. The cell lysates were subjected to immunoprecipitation analysis with anti-FLAG antibodies followed by immunoblotting with anti-Myc antibodies. $Ub_n$, polyubiquitinated; *DMSO*, $Me_2SO$.

A172-Pin1i cells demonstrate a more prominent induction of the Daxx protein upon $H_2O_2$ treatment, compared with control cells (Fig. 3*A*). Following this enhanced Daxx induction, the phosphorylation of both ASK1 and JNK, indicating activation, was consistently increased in A172-Pin1i cells compared with control cells (Fig. 3*A*). Furthermore, the levels of cleaved caspase-3 and cleaved PARP, indicating apoptosis, were observed to be significantly higher in Pin1-depleted cells (Fig. 3*A*), consistent with data from our TUNEL analysis (Fig. 2*D*). An *in vitro* kinase assay further demonstrated that JNK activity was significantly increased in A172-Pin1i cells following $H_2O_2$ treatment when compared with the control cells (Fig. 3*B*). These results indicate that the inhibition of Pin1 may sensitize the cells to the apoptotic response induced by $H_2O_2$ by augmenting the induction and activation of the Daxx-ASK1-JNK pathway. To confirm this possibility, we transduced Daxx-specific siRNA oligonucleotides to block endogenous Daxx expression as well as treated the cells in parallel experiments with the JNK inhibitor II (SP600125). We found that either Daxx siRNA or SP600125 treatment could significantly reduce the susceptibility of A172-Pin1i cells to $H_2O_2$-induced cellular apoptosis (Fig. 3, *C* and *D*). This indicates that the targeted depletion of Pin1 enhances the induction of Daxx, thereby augmenting the apoptotic response via the ASK1/JNK pathway upon oxidative stress.

*Pin1 Facilitates the Degradation of Daxx via the Ubiquitin-Proteasome Pathway*—Since the depletion of Pin1 was found to enhance the expression of Daxx following oxidative stress, we speculated whether the corollary would be true, such that high levels of Pin1 might in fact inhibit the expression of Daxx. To test this possibility, we initially co-transfected A172 cells with FLAG-tagged Daxx and Pin1 and then examined the expression levels of Daxx. Immunoblotting analysis demonstrated that Pin1 reduces the exogenously transduced FLAG-Daxx levels in a dose-dependent manner (Fig. 4*A*). Moreover, the expression levels of endogenous Daxx were also found to be reduced in these Pin1-overexpressed cells (Fig. 4*B*). Interestingly, the mRNA levels of Daxx are not altered upon Pin1 overexpression (data not shown), indicating that Pin1 might affect the protein stability of Daxx.

To address whether either the binding or the catalytic activity of Pin1 is required for the suppression of Daxx, we performed a parallel experiment using either a WW domain (binding domain) mutant (W34A) or PPIase domain (catalytic domain) mutant (K63A) of Pin1. Neither of these mutants fully down-regulate FLAG-Daxx expression (Fig. 4*C*), indicating that both the WW and PPIase domains are indeed required for this function of Pin1.

We next performed parallel experiments with or without $H_2O_2$ treatment. Pin1 overexpression was found to suppress Daxx expression in both untreated and $H_2O_2$-treated cells (Fig. 4*D*), indicating that Pin1 affects Daxx expression independently of $H_2O_2$ exposure.

Cycloheximide analysis also revealed that the protein stability of both endogenously and exogenously expressed Daxx is significantly reduced when Pin1 is overexpressed (Fig. 4, *E* and *F*), further indicating that Pin1 enhances the degradation of Daxx. To address whether this is mediated by the ubiquitin-proteasome pathway, we performed parallel experiments using the proteasome inhibitors MG132 and MG115. Treatment with these inhibitors significantly inhibited the degradation of Daxx following Pin1 overexpression (Fig. 4*G*). Moreover, immunoprecipitation analysis with cells co-transfected with FLAG-Daxx and Myc-ubiquitin, with or without Pin1 co-transfection, further revealed that Pin1 overexpression significantly enhances the polyubiquitination of the Daxx protein (Fig. 4*H*). Furthermore, the reciprocal ubiquitination analysis with or without $H_2O_2$ treatment further revealed that Pin1 enhances the polyubiquitination of Daxx irrespective of $H_2O_2$ exposure (Fig. 4*I*). These results together confirm that Pin1 enhances the degradation of the Daxx protein via the ubiquitin-proteasome pathway independently of proapoptotic stimuli, such as $H_2O_2$ treatment.

*Pin1 Interacts with Daxx Phosphorylated on Its Ser$^{178}$-Pro Motif*—Our previous results indicated that Pin1 could affect the protein stability of Daxx by mediating the ubiquitination status of this protein. We next examined whether Pin1 could directly interact with Daxx. Immunoprecipitation analysis revealed that this is indeed the case (Fig. 5*A*). GST pull-down analyses further demonstrated that wild-type Pin1 binds the Daxx protein but that the Pin1 WW domain mutant W34A does not (Fig. 5*B*). The association between Pin1 and Daxx was also found to be completely abolished by pretreatment of the cell lysates with calf intestine alkaline phosphatase prior to the GST pull-down analysis (Fig. 5*C*), indicating that Pin1 binds only phosphorylated Daxx. Interestingly, the interaction between Pin1 and Daxx could be observed in both the absence and the presence of $H_2O_2$ stimulation (Fig. 5*B*), indicating that this interaction is independent of the corresponding stress response and that the Pin1 binding motif in Daxx may be constitutively phosphorylated in these cells.

Immunofluorescence analysis further demonstrated that Pin1 co-localizes with Daxx in intranuclear aggregates corresponding to promyelocytic leukemia bodies in the absence of $H_2O_2$ stimulation, as reported previously (11) (Fig. 5*D*). Upon $H_2O_2$ stimulation, certain subsets of both Daxx and Pin1 were found to translocate diffusely into the cytoplasm, although the majority of these proteins were still retained in the nucleus and colocalized together in nuclear bodies (Fig. 5*D*).

To identify the specific Pin1 binding site in the Daxx protein, we created several Daxx deletion mutants and performed GST pull-down analysis. These experiments revealed that an N-terminal Daxx deletion mutant (Δ1–36) could still bind Pin1 but also that an extended N-terminal deletion mutant (Δ1–183)

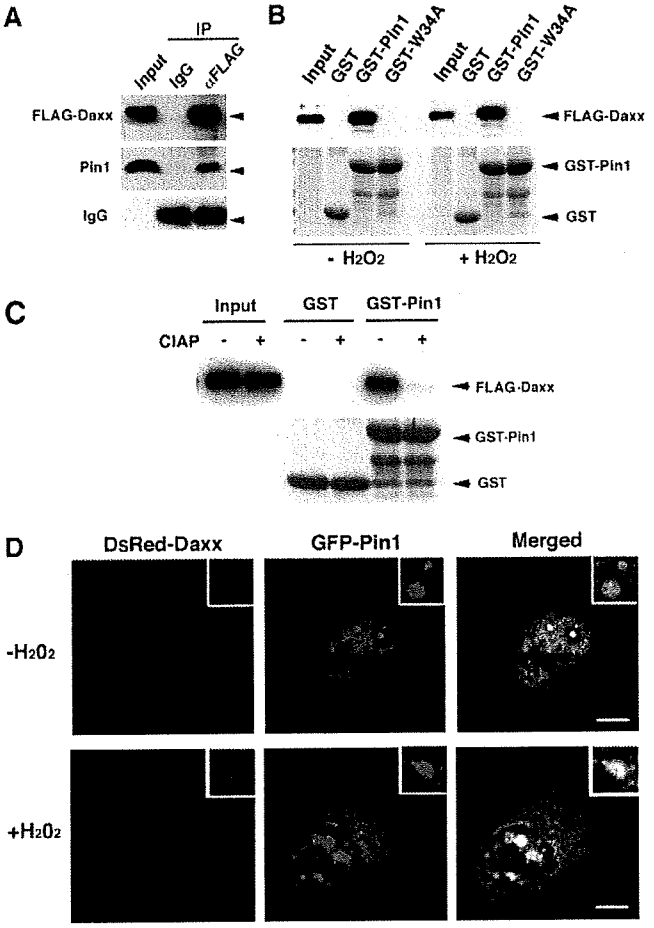


FIGURE 5. **Pin1 interacts with phosphorylated Daxx.** *A*, 293T cells were transfected with FLAG-Daxx and Pin1. After 24 h, cell lysates were subjected to immunoprecipitation (*IP*) analysis with anti-FLAG or nonimmunized IgG followed by immunoblotting analysis with anti-FLAG or anti-Pin1 antibodies. *B*, 293T cells were transfected with FLAG-Daxx. After 24 h, cell lysates were subjected to GST pull-down analysis with GST, GST-Pin1, or GST-Pin1W34A mutant followed by immunoblotting with anti-FLAG antibody. *C*, cell lysates derived from 293T cells transfected with FLAG-Daxx were treated or untreated with calf intestine alkaline phosphatase (*CIAP*), followed by GST pull-down analysis as described in *B*. *D*, HeLa cells were co-transfected with GFP-Pin1 and Ds-Red-Daxx. After 24 h, the cells were treated or untreated with $H_2O_2$ for 3 h. Cells were then fixed and stained with 4′,6-diamino-2-phenylindole (*DAPI*) and then subjected to confocal microscopy. *Scale bar*, 10 μm.

failed to do so (Fig. 6*A*). These data indicate that Pin1 binds to Daxx in the region between amino acids 36 and 183.

Previous reports have indicated that Pin1 can bind only phosphorylated Ser/Thr-Pro motifs (4, 5). Since there is only a single Ser/Thr-Pro motif (Ser$^{178}$-Pro) between residues 36 and 183 in the Daxx protein, we created a Daxx site-directed mutant at this site by substituting the serine 178 with alanine (S178A). Moreover, we created an additional Daxx mutant by substitution of serine 668 with alanine (S668A), since this site has been shown to be phosphorylated (14). Both GST pull-down and immunoprecipitation analyses subsequently revealed that Pin1 binds both wild-type and the S668A mutant Daxx proteins but not the S178A mutant (Fig. 6, *B* and *C*). These results confirm that Pin1 indeed binds the phosphorylated Ser$^{178}$-Pro motif of Daxx.

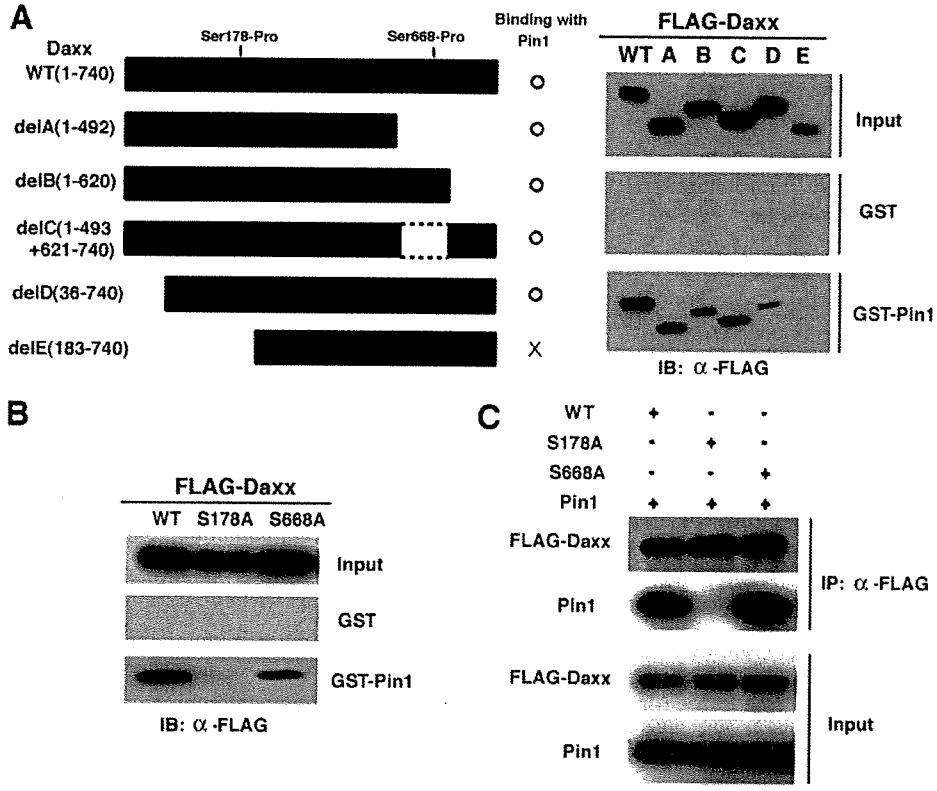


FIGURE 6. **Pin1 interacts with Daxx via its Ser$^{178}$-Pro motif.** *A* (*left*), schematic representation of the Daxx deletion mutants generated in this study. *Right*, 293T cells were transfected with the indicated Daxx-deletion mutants for 24 h. Cell lysates were then subjected to GST pull-down followed by immunoblotting analysis. *B*, 293T cells were transfected with the indicated Daxx site-directed mutants and subjected to GST pull-down analysis as shown in *A*. *C*, 293T cells were co-transfected with the indicated Daxx constructs. At 24 h following transfection, the cells were treated with the proteasome inhibitors MG132 and MG115 (10 $\mu$M each). After 12 h, cell lysates were harvested and subjected to immunoprecipitation analysis with anti-FLAG antibodies followed by immunoblotting analysis with the indicated antibodies. *WT*, wild type.

*The Daxx-S178A Mutant Is Refractory to Pin1-mediated Degradation and Shows Strong Proapoptotic Properties*—To further examine the functional interactions between Pin1 and Daxx, we initially investigated the nature of the S178A mutant in terms of its protein stability. Cycloheximide analysis revealed that the S178A Daxx mutant is resistant to degradation following the co-transfection of Pin1 (Fig. 7*A*). Consistent with this result, this S178A mutant also shows lower levels of ubiquitination compared with wild-type Daxx upon Pin1 co-transfection (Fig. 7*B*). A reciprocal immunoprecipitation analysis further revealed that the S178A mutant was refractory to be polyubiquitinated following Pin1 overexpression as compared with wild-type Daxx (Fig. 7*C*). These results together confirm that the direct interaction between Pin1 and Daxx via the Ser$^{178}$-Pro motif augments the ubiquitination of Daxx and thereby enhances its degradation by the proteasome.

We next examined the proapoptotic properties of the S178A Daxx mutant in the absence or presence of exogenous Pin1. A previous report has indicated that the co-transfection of Daxx and its downstream target ASK1 initiates apoptosis in HeLa cells (22). We therefore co- transfected HeLa cells with ASK1 and either FLAG-Daxx or S178A Daxx in the presence or absence of Pin1. As shown in Fig. 7, *D* and *E*, the co-transfection of ASK1 with either wild-type or S178A mutant Daxx results in cellular apoptosis. However, the S178A mutant shows stronger proapoptotic effects compared with wild type Daxx. Furthermore, when co-transfected with Pin1, the S178A mutant still retains its potent ability to induce cellular apoptosis, which is in contrast to wild-type Daxx, which fails to induce apoptosis in the presence of high levels of Pin1, as revealed by either immunostaining for cleaved caspase-3 or Hoechst 33258 staining for apoptotic nuclei (Fig. 7, *D* and *E*). These results together indicate that the proapoptotic properties of the S178A mutant are refractory to the anti-apoptotic function of Pin1.

*Reverse Correlation between Pin1 and Daxx Expression in Human Glioblastoma Tissues*—To further examine the pathological role of Pin1 in the degradation of Daxx, we determined the expression levels of the Daxx protein in the 28 grade 4 human glioblastoma tissues that we analyzed earlier for Pin1 expression by immunohistochemical staining. As shown in Fig. 1, Pin1 is expressed to various degrees in human glioblastoma tissues. Consistent with our molecular data, we found that Daxx staining was predominantly absent in glioma tissues containing high levels of Pin1 and that Daxx accumulation in the nucleus was evident in cases containing relatively low expression levels of Pin1 (Fig. 8*A*). Among the 28 grade 4 human glioblastoma tissues that we examined, there was also a significant reverse correlation between Pin1 expression and the immunoreactivity of Daxx, as determined by the Spearman rank correlation test ($p < 0.01$) (Fig. 8*B*). These results further support the notion that Pin1 is important for the regulation of Daxx expression *in vivo* and strengthen the significance of Pin1 overexpression in the negative regulation of Daxx in malignant human glioma.

## DISCUSSION

In our current study, we report that the peptidyl-prolyl isomerase Pin1 associates with phosphorylated Daxx and enhances its degradation, resulting in the prevention of oxidative stress-induced cellular apoptosis. We find that 1) Pin is highly overexpressed in human gliomas, and its expression levels parallel the malignant properties of the glioma cells; 2) Pin1-depleted A172 glioblastoma cells are highly susceptible to cellular apoptosis induced by either hydrogen peroxide or stimulatory Fas antibodies; 3) Pin1 inhibition enhances the induction of Daxx and the activation of the ASK1/JNK apoptotic pathway; 4) Pin1 overexpression causes the rapid degradation of the Daxx protein via the ubiquitin-proteasome pathway; 5) Pin1 interacts with Daxx via its phosphorylated Ser$^{178}$-Pro

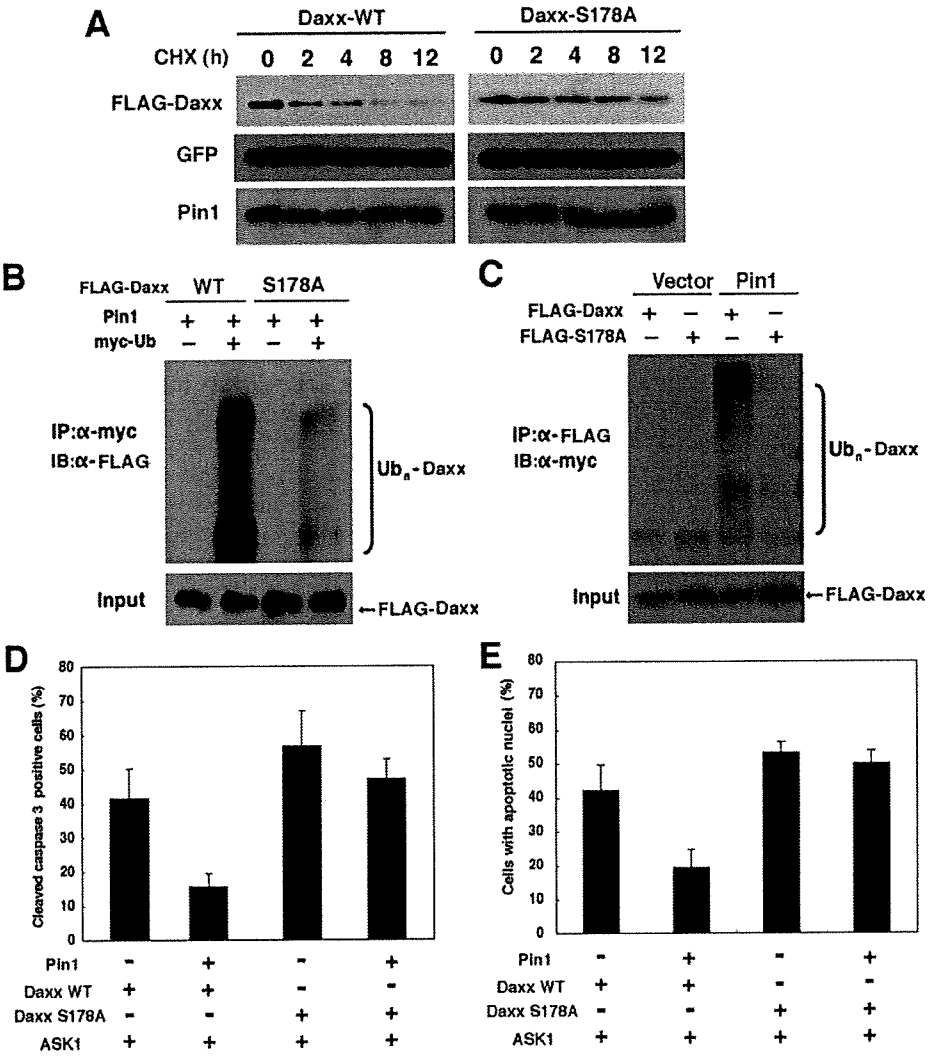


FIGURE 7. **The Daxx-S178A mutant is refractory to Pin1-mediated degradation and shows strong pro-apoptotic properties in the presence of Pin1.** *A*, 293T cells were co-transfected with the indicated constructs. After 24 h, cells were treated with CHX and harvested at the indicated time points followed by immunoblotting analysis. *B*, 293T cells were co-transfected with the indicated vectors. At 24 h following transfection, the cells were treated with the proteasome inhibitors MG132 and MG115 (10 $\mu$M each). After 12 h, cell lysates were harvested and subjected to immunoprecipitation (*IP*) analysis with anti-Myc antibodies followed by immunoblotting (*IB*) with anti-FLAG antibodies. *C*, 293T cells were co-transfected with the indicated vectors. At 24 h following transfection, the cells were treated with the proteasome inhibitors MG132 and MG115 (10 $\mu$M each). After 12 h, cell lysates were harvested and subjected to immunoprecipitation analysis with anti-FLAG antibodies followed by immunoblotting with anti-Myc antibodies. *D* and *E*, HeLa cells were co-transfected with ASK1 and either wild-type Daxx or its S178A mutant and co-transfected with either GFP or GFP-Pin1. After 30 h, the cells were fixed and subjected to immunofluorescent analysis with anti-cleaved caspase-3 antibodies followed by the Hoechst 33258 staining. The relative apoptotic cell numbers are scored by counting 200 GFP-positive cells with either caspase-3-positive (*D*) or apoptotic (*E*) nuclei by Hoechst 33258 staining. *WT*, wild type.

motif, and the Daxx-S178A mutant is refractory to both Pin1-mediated degradation and the anti-apoptotic effects of Pin1; and 6) there is a significant reverse correlation between the expression of Pin1 and Daxx in human glioblastoma tissues. These results are the first to demonstrate that Pin1-mediated prolyl isomerization plays a crucial role in the post-translational regulation of Daxx. Furthermore, we have shown that Pin1 significantly suppresses the Daxx-mediated apoptotic response in human glioma cells as a potent antiapoptosis factor.

Cancer cells often exhibit several types of malignant behavior, including a self-sufficiency in terms of growth signals, insensitivity to growth-inhibitory signals, and the ability to evade programmed cell death (1). One of the current major issues in the clinical treatment of human glioma is the resistance of many of these tumors to chemotherapy (2). In our current report, however, we show that Pin1 inhibition increases the sensitivity of glioma cells to both $H_2O_2$ and Fas-mediated apoptosis and that this is accompanied by the increased expression of Daxx. In contrast, Pin1 overexpression significantly suppresses the expression of Daxx, thereby enhancing its degradation via the ubiquitin-proteasome pathway. These data suggest that aberrantly high levels of Pin1 in tumor cells can contribute to a blockade of proapoptotic pathways and promote the inappropriate survival of tumor cells. The inhibition of Pin1 may therefore be an effective strategy for the future treatment of glioma.

The involvement of Pin1 in cellular apoptosis has been addressed previously. First, Pin1 has been shown to interact with both p53 and p73, thereby affecting their stability. This modifies both the cell cycle-regulatory mechanisms and apoptotic pathways induced by genotoxic stress stimuli (23–25). Second, Pin1 also binds the antiapoptotic protein Bcl-2 during mitosis at a proline-rich loop region, thereby blocking its cytoprotective and ion channel-forming activities (26). Pin1 has also been reported to interact with the BH3-only protein BIMEL, thus inducing apoptosis in neurons (27). These results indicate multiple effects of Pin1 on cellular apoptosis in different tissues or cell types via its interaction with specific substrate proteins. However, given that the Daxx-ASK1-JNK pathway plays a crucial role in cellular apoptosis by various proapoptotic stimuli and that this signaling pathway is often deregulated in many human tumors (10), our current study uncovers an important molecular mechanism by which malignant tumor cells with aberrantly high Pin1 levels could evade Daxx-mediated apoptosis. This in turn could directly contribute to tumor expansion and resistance to anticancer therapies.

It has been suggested that the subcellular localization of Daxx might determine its activity and function toward the induction of proapoptotic signaling, and this is critically regulated by multiple related factors. Several lines of evidence have now indi-

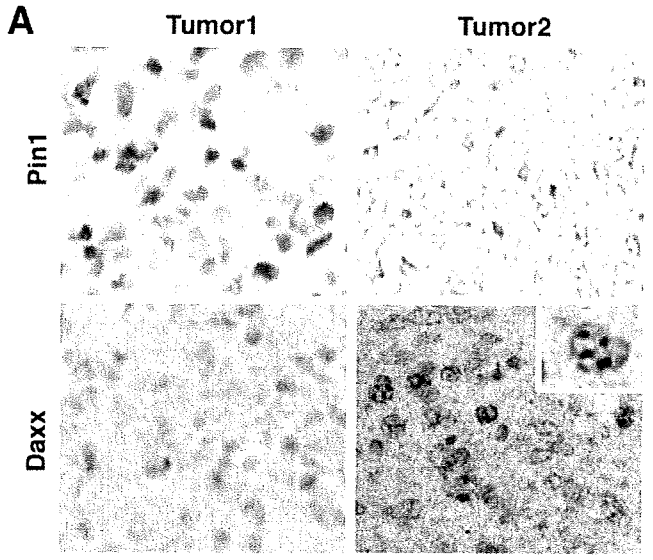


B

| | Pin1 expression | | | |
|---|---|---|---|---|
| Daxx expression | Low level (n=3) | High level (n=15) | Very high level (n=10) | Total |
| Positive | 3(10.7%) | 7(25%) | 0(0%) | 10(35.7%) |
| Negative | 0(0%) | 8(28.6%) | 10(35.7%) | 18(64.3%) |
| Total | 3(10.7%) | 15(53.6%) | 10(35.7%) | 28(100%) |

FIGURE 8. **Reverse correlation between Pin1 and Daxx expression in human glioblastoma tissues.** *A*, human glioblastoma tissues were stained with anti-Daxx or anti-Pin1 antibody followed by staining with diaminobenzene (DAB; *brown*). *Left*, a representative tumor showing strong staining for Pin1 and negative Daxx staining; *right*, a representative low Pin1-stained glioma with an accumulation of Daxx in the nucleus. Nuclei were stained weakly with hematoxylin. *Inset*, a focal magnification of Daxx staining in nuclear bodies. *B*, a summary of immunohistochemical analysis of a 28-human glioblastoma tissue panel is shown. The levels of Pin1 and Daxx expression were determined, and a significant reverse correlation was confirmed using a Spearman rank test ($p < 0.01$).

cated that Daxx might relocalize from the nucleus to the cytoplasm upon receipt of specific stimuli, including Fas stimulation, oxidative stresses, and glucose deprivation (10, 14). The regulation of Daxx nuclear export appears to be dependent on its phosphorylation on $Ser^{668}$, potentially mediated by the HIPK1 kinase (14). This in turn enhances the interaction of Daxx with the nuclear exporter CRM1, which controls its phosphorylation-dependent translocation to the cytoplasm (14). DJ-1 and heat shock protein 27 (HSP27) have been shown to be Daxx suppressor proteins that can directly interact with Daxx and suppress its nuclear export by CRM1, thereby inhibiting ASK1/JNK activation and apoptosis (28, 29). However, our current study has revealed for the first time that in addition to its phosphorylation at the C-terminal $Ser^{668}$ residue, Daxx is also phosphorylated on $Ser^{178}$ and subsequently targeted by Pin1-mediated prolyl isomerization for degradation via the ubiquitin-proteasome pathway.

The ubiquitin-mediated proteolysis of Daxx has been reported recently. Daxx has been shown to undergo ubiquitination and degradation in response to double strand DNA damage, resulting in the translocation of Ras-association domain family 1C (RASSF1C) to the microtubules (30). Moreover, BTB domain-containing speckle-type POZ protein serves as an adaptor of Daxx that facilitates its ubiquitination by Cul3-based ubiquitin ligase (31). However, these studies did not reveal any details regarding the mechanistic processes underlying the ubiquitination of Daxx following the receipt of proapoptotic stimuli. It is possible that Pin1-mediated prolyl isomerization of Daxx on phosphorylated $Ser^{178}$-Pro, as shown in this study, might affect these ubiquitination processes as they pertain to Daxx.

Our current data also clearly show that both the Pin1 WW domain and PPIase domain are required for the degradation of Daxx, suggesting that the prolyl isomerization of Daxx by Pin1 is important for its polyubiquitination and degradation. Our current findings thus provide the first evidence that Daxx protein stability is regulated by a series of post-translational modifications (*i.e.* phosphorylation and subsequent prolyl isomerization leading to ubiquitination). The future identification of the kinase(s) responsible for phosphorylation of the $Ser^{178}$-Pro Pin1 binding motif of Daxx might further uncover the mechanisms underlying antiapoptotic signaling in tumor cells.

In summary, we demonstrate herein that Pin1 is a negative regulator of Daxx and demonstrate a novel regulatory mechanism of Daxx involving phosphorylation-dependent prolyl isomerization. The targeted inhibition of Pin1 could therefore be a valid therapeutic strategy to induce cellular apoptosis in malignant tumors. This includes gliomas in which aberrantly high Pin1 expression is often observed.

*Acknowledgments—We thank H. Soeda, A. Okayama, and N. Takizawa for technical assistance.*

## REFERENCES

1. Hanahan, D., and Weinberg, R. A. (2000) *Cell* **100,** 57–70
2. Bremer, E., van Dam, G., Kroesen, B. J., de Leij, L., and Helfrich, W. (2006) *Trends Mol. Med.* **12,** 382–393
3. Rodriguez-Nieto, S., and Zhivotovsky, B. (2006) *Curr. Pharm. Des.* **12,** 4411–4425
4. Lu, K. P., Liou, Y. C., and Zhou, X. Z. (2002) *Trends Cell Biol.* **12,** 164–172
5. Ryo, A., Liou, Y. C., Lu, K. P., and Wulf, G. (2003) *J. Cell Sci.* **116,** 773–783
6. Ryo, A., Suizu, F., Yoshida, Y., Perrem, K., Liou, Y. C., Wulf, G., Rottapel, R., Yamaoka, S., and Lu, K. P. (2003) *Mol. Cell* **12,** 1413–1426
7. Ryo, A., Nakamura, M., Wulf, G., Liou, Y. C., and Lu, K. P. (2001) *Nat. Cell Biol.* **3,** 793–801
8. Ryo, A., Uemura, H., Ishiguro, H., Saitoh, T., Yamaguchi, A., Perrem, K., Kubota, Y., Lu, K. P., and Aoki, I. (2005) *Clin. Cancer Res.* **11,** 7523–7531
9. Yang, X., Khosravi-Far, R., Chang, H. Y., and Baltimore, D. (1997) *Cell* **89,** 1067–1076
10. Salomoni, P., and Khelifi, A. F. (2006) *Trends Cell Biol.* **16,** 97–104
11. Torii, S., Egan, D. A., Evans, R. A., and Reed, J. C. (1999) *EMBO J.* **18,** 6037–6049
12. Li, H., Leo, C., Zhu, J., Wu, X., O'Neil, J., Park, E. J., and Chen, J. D. (2000) *Mol. Cell Biol.* **20,** 1784–1796
13. Khelifi, A. F., D'Alcontres, M. S., and Salomoni, P. (2005) *Cell Death Differ.* **12,** 724–733
14. Song, J. J., and Lee, Y. J. (2004) *J. Biol. Chem.* **279,** 30573–30578
15. Sasaki, T., Ryo, A., Uemura, H., Ishiguro, H., Inayama, Y., Yamanaka, S., Kubota, Y., Nagashima, Y., Harada, M., and Aoki, I. (2006) *Pathol. Res. Pract.* **202,** 357–364
16. Ryo, A., Togo, T., Nakai, T., Hirai, A., Nishi, M., Yamaguchi, A., Suzuki, K., Hirayasu, Y., Kobayashi, H., Perrem, K., Liou, Y. C., and Aoki, I. (2006) *J. Biol. Chem.* **281,** 4117–4125
17. Tsuruta, F., Masuyama, N., and Gotoh, Y. (2002) *J. Biol. Chem.* **277,** 14040–14047
18. Yamamoto, K., Ichijo, H., and Korsmeyer, S. J. (1999) *Mol. Cell Biol.* **19,**

8469–8478
19. Wulf, G. M., Ryo, A., Wulf, G. G., Lee, S. W., Niu, T., Petkova, V., and Lu, K. P. (2001) *EMBO J.* **20,** 3459–3472
20. Guha, A., and Mukherjee, J. (2004) *Curr. Opin. Neurol.* **17,** 655–662
21. Duan, L., Aoyagi, M., Tamaki, M., Yoshino, Y., Morimoto, T., Wakimoto, H., Nagasaka, Y., Hirakawa, K., Ohno, K., and Yamamoto, K. (2004) *Clin. Cancer Res.* **10,** 234–243
22. Chang, H. Y., Nishitoh, H., Yang, X., Ichijo, H., and Baltimore, D. (1998) *Science* **281,** 1860–1863
23. Mantovani, F., Piazza, S., Gostissa, M., Strano, S., Zacchi, P., Mantovani, R., Blandino, G., and Del Sal, G. (2004) *Mol. Cell* **14,** 625–636
24. Zheng, H., You, H., Zhou, X. Z., Murray, S. A., Uchida, T., Wulf, G., Gu, L., Tang, X., Lu, K. P., and Xiao, Z. X. (2002) *Nature* **419,** 849–853
25. Zacchi, P., Gostissa, M., Uchida, T., Salvagno, C., Avolio, F., Volinia, S., Ronai, Z., Blandino, G., Schneider, C., and Del Sal, G. (2002) *Nature* **419,** 853–857
26. Pathan, N., Aime-Sempe, C., Kitada, S., Basu, A., Haldar, S., and Reed, J. C. (2001) *Neoplasia* **3,** 550–559
27. Becker, E. B., and Bonni, A. (2006) *Neuron* **49,** 655–662
28. Junn, E., Taniguchi, H., Jeong, B. S., Zhao, X., Ichijo, H., and Mouradian, M. M. (2005) *Proc. Natl. Acad. Sci. U. S. A.* **102,** 9691–9696
29. Charette, S. J., Lavoie, J. N., Lambert, H., and Landry, J. (2000) *Mol. Cell Biol.* **20,** 7602–7612
30. Kitagawa, D., Kajiho, H., Negishi, T., Ura, S., Watanabe, T., Wada, T., Ichijo, H., Katada, T., and Nishina, H. (2006) *EMBO J.* **25,** 3286–3297
31. Kwon, J. E., La, M., Oh, K. H., Oh, Y. M., Kim, G. R., Seol, J. H., Baek, S. H., Chiba, T., Tanaka, K., Bang, O. S., Joe, C. O., and Chung, C. H. (2006) *J. Biol. Chem.* **281,** 12664–12672

# 5

# Methods for High-Throughput Materialization of Genetic Information Based on Wheat Germ Cell-Free Expression System

Tatsuya Sawasaki, Ryo Morishita, Mudeppa D. Gouda, and Yaeta Endo

## Summary

Among the cell-free protein synthesis systems, the wheat germ-based translation system has significant advantages for the high-throughput production of eukaryotic multidomain proteins in folded state. Here, we describe protocols for this cell-free expression system.

**Key Words:** Cell-free protein synthesis; wheat germ extract; 5'- and 3'-UTRs; PCR; using split-primers; transcription and translation; purification of products.

## 1. Introduction

This chapter describes in detail the methods for high-throughput protein production based on the cell-free system prepared from eukaryotic wheat embryos. The methods are divided into four steps as follows: (1) preparation of the highly efficient extract from wheat embryos; (2) generation of DNA template for transcription of the desired open reading frame (ORF) with or without cloning; (3) sequential transcription-trans-

From: *Methods in Molecular Biology*, vol. 375,
*In Vitro Transcription and Translation Protocols, Second Edition*
Edited by: G. Grandi © Humana Press Inc., Totowa, NJ

lation by using PCR generated DNA or highly purified plasmid carrying ORF based on the bilayer reaction method, and (4) purification of synthesized protein by on-column digestion. Purification of in vitro-transcribed products is successfully carried out by synthesizing the proteins as fused forms and exploiting the fused tag. Finally, the tag is removed proteolytically. This platform is already in use for functional and structural analyses of gene products *(1,2)*.

## 2. Materials

1. Wheat seeds.
2. Roter Speed Mill (model pulverisette 14, Fritsh, Germany).
3. Sieve (710- to 850-μm mesh).
4. Cyclohexane and carbon tetrachloride.
5. Nonidet P-40.
6. Milli-Q water, freshly prepared.
7. Bronson model 2210 sonicator (Yamato, Japan).
8. Extraction buffer: 40 m*M* HEPES-KOH, pH 7.6, 100 m*M* potassium acetate, 5 m*M* magnesium acetate, 2 m*M* calcium chloride, 4 m*M* DTT, and 0.3 m*M* of each of the 20 amino acids.
9. Sephadex G-25 (fine) (Amersham Biosciences).
10. pEU protein expression vector.
11. cDNA of protein to be synthesized.
12. Oligonucleotide primers.
13. PCR thermo-cycler MP (Takara, Otsu, Japan).
14. ExTaq DNA polymerase (Takara).
15. 5X Transcription buffer (TB): 400 m*M* HEPES-KOH, pH 7.8, 80 m*M* magnesium acetate, 10 m*M* spermidine, and 50 m*M* DTT.
16. Nucleotide tri-phosphates (NTPs) mix: a solution containing ATP, GTP, CTP, and UTP (25 m*M* each).
17. SP6 RNA polymerase and RNasin (80 U/μL, Promega, Madison, WI).
18. Microcon (YM-50; Millipore, Bedford, MA).
19. Amicon Ultra-15 (10 K, Millipore, cat. no., UFC901024).
20. 2 mg/mL (20 mg/mL for large-scale production) creatine kinase.
21. Translational substrate buffer (TSB): 30 m*M* HEPES-KOH, pH 7.8, 100 m*M* potassium acetate, 2.7 m*M* magnesium acetate, 0.4 m*M* spermidine, 2.5 m*M* DTT, 0.3 m*M* amino acid mix, 1.2 m*M* ATP, 0.25 m*M* GTP, and 16 m*M* creatine phosphate.

22. 24-Well microplate (Whatman Inc., Clifton, NJ) for small-scale production or 6-well microplate (Whatman Inc.) for large-scale production.
23. 1X PBS: 140 m*M* NaCl, 2.7 m*M* KCl, 10.1 m*M* $Na_2PO_4$, 1.8 m*M* $KH_2PO_4$.
24. Poly-Prep Chromatography Column (Bio-Rad, cat. no. 731-1550).
25. Glutathione Sepharose 4B (Amersham Biosciences).
26. PreScission Protease (2 U/μL, Amersham Biosciences).

## 3. Methods

### 3.1. Preparation of Wheat Embryos Extract

Isolation of embryos and preparation of extract were carried out as reported previously.*(3)*. The main aim is to remove contaminating endosperms from embryos by washing (**Subheading 3.1.1., steps 5** and **6**).

#### 3.1.1. Isolation of Wheat Embryo

1. Grind the wheat seeds in a mill (Roter Speed Mill).
2. Sieve through a 710- to 850-μm mesh.
3. Select the intact embryos by solvent flotation using cyclohexane and carbon tetrachloride as solvents (1:2.5 v/v).
4. Dry overnight in a fume hood.
5. Wash three times with 10 vol of sterile water under vigorous stirring.
6. Sonicate for 3 min in a 0.5% Nonidet P-40 solution by using a Bronson model 2210 sonicator.

#### 3.1.2. Preparation of Wheat Embryo Extract

1. Grind 5 g of isolated wheat embryo to a fine powder in liquid nitrogen.
2. Add 5 mL of extraction buffer and vortex the mixture briefly.
3. Centrifuge the embryo lysate (30,000*g*; 30 min) and retain the supernatant.
4. Gel-filtrate the supernatant by using a sephadex G-25 (fine) column, equilibrated with 2 vol of extraction buffer.
5. Replace the ingredients by the gel-filtration as above but using the TSB as equilibration buffer.
6. Collect the void fraction.
7. Concentrate the fraction to approx 1/3 vol using Amicon Ultra-15 (10 K) filter unit according to the manufacturer's instructions at 10°C.
8. Adjust to 240 A260/mL with the TBS.
9. Divide into small aliquots, and store at –80°C until use.